GAW Report No. 179

Intercomparison of Global UV Index from Multiband Filter Radiometers: Harmonization of global UVI and spectral irradiance

For more information, please contact:

World Meteorological Organization

Research Department

Atmospheric Research and Environment Branch

7 *bis*, avenue de la Paix – P.O. Box 2300 – CH 1211 Geneva 2 – Switzerland

Tel.: +41 (0) 22 730 83 14 – Fax: +41 (0) 22 730 80 27

E-mail: cpa@wmo.int – Website: http://www.wmo.int/pages/prog/arep/index_en.html

World Meteorological Organization

Weather • Climate • Water

WMO/TD - No. 1454

Chairperson, Publications Board
World Meteorological Organization (WMO)
7 *bis* avenue de la Paix
P.O. Box No. 2300
CH-1211 Geneva 2, Switzerland

Tel.: +41 22 730 8403
Fax.: +41 22 730 8040
E-mail: publications@wmo.int

WORLD METEOROLOGICAL ORGANIZATION
GLOBAL ATMOSPHERE WATCH

INTERCOMPARISON of GLOBAL UV INDEX from MULTIBAND FILTER RADIOMETERS: HARMONIZATION of GLOBAL UVI and SPECTRAL IRRADIANCE

Authors

Bjørn Johnsen, Berit Kjeldstad, Tommy Nakken Aalerud, Lill Tove Nilsen, Josef Schreder, Mario Blumthaler, Germar Bernhard, Chrysanthi Topaloglou, Outi Meinander, Asadollah Bagheri, James R. Slusser and John Davis

The Research Council of Norway

Statens strålevern
Norwegian Radiation Protection Authority

COST

WMO/TD-No. 1454

Table of Contents

Preface

The intercomparison of global UVI from multiband filter radiometers in Oslo May 2005 was initiated from a national project, Factors Affecting UV Radiation in Norway (FARIN), funded by the Norwegian Research Council. The project involves UV monitoring and quality assurance of multiband filter radiometers (MBFR) operating in the Norwegian network. Support from WMO and COST726 made it possible to extend the campaign with radiometers representing several UV networks in Europe, in addition to two networks in the United States. The spectroradiometer reference group could be extended to four spectroradiometers, with one instrument closely linked to the QASUME European reference instrument, used for the harmonization of spectral UV measurements in Europe. Scientific missions involved representatives from Greece and Poland.

The present intercomparison of MBFRs was conducted as an international venture, co-organized by the Norwegian Radiation Protection Authority (NRPA), the Norwegian University of Science and Technology (NTNU), the Norwegian Institute for Air Research (NILU), the World Meteorological Organization (WMO) and the EC COST-726 action. Groups from all around the world were invited to join the arrangement. Forty-three MBFRs took part, representing measurement sites and networks from Antarctica to the Arctic, North and South America, Africa, Europe and Nepal. The Austrian company CMS Ing. Dr Schreder GmbH was hired to bring and operate a high-resolution and well-characterized spectroradiometer. This radiometer provides a link to several earlier international intercomparisons of spectroradiometers and broadband meters.

Abstract

Multiband filter radiometers (MBFRs) are extensively used in national networks for UV climate monitoring and information to the public about the potential risks of solar UV exposure. In order to provide an international, uniform expression of measurement results, harmonized calibration scales are needed. In this paper we present the results of the first large-scale international intercomparison of MBFRs held in Oslo in 2005. In total 43 MBFRs and four high-resolution spectroradiometers were assembled, representing UV monitoring stations from Antarctica to the Arctic, North and South America, Africa, Europe and Nepal (Kathmandu). The MBFRs were spectrally characterized in the laboratory and intercompared outdoors against a group of spectroradiometers. Based on the MBFR's individual characteristics retrieved during the calibration campaign, a set of harmonized data products were constructed for individual radiometers: Global UV index, spectral irradiance at standard wavelengths in the UVB and UVA corresponding to 1nm bandwidth (FWHM), UVA cloud optical depth and total ozone amount. This information was provided to all users. A blind intercomparison of the UV index provided by the participants was conducted against a set of reference data. For the 8 to 18 day core-period, the set of 26 data supplied by the users agreed within ±12% (2σ) for solar zenith angles (SZA) ≤ 80º. The set of harmonized UVI for 33 MBFRs operating in the same period agreed within ≤ ±5% (2σ) for SZAs ≤ 90º. A group of six additional MBFRs operating shortly after the core-period agreed within ±7% (2σ) and a group of four MBFRs operating in the autumn, traceable to the same reference, agreed within ±5% (2σ). The results demonstrated that MBFRs of type GUV, NILU-UV and UV-MFRSR-7 may provide highly accurate measurements of UV index for all realistic sky conditions and SZAs. The results are traceable to the European QASUME reference spectroradiometer.

1. INTRODUCTION

Multiband filter radiometers (MBFRs) are presently operating as stand-alone radiometers or within UV-monitoring networks on almost all continents, though they are less numerous than broadband radiometers. A strong motivation behind the implementation of UV monitoring networks is to provide information to the public and scientific communities about the level of harmful UV radiation at the Earth's surface. The Global Solar UV index (UVI) [*WHO, 2002*] is an important tool for raising public awareness and for alerting the people about the need to take protective measures when exposed to UV. The unit is based on the CIE erythema action spectrum [*McKinlay and Diffey, 1987; ISO, 1999*] and has been internationally adopted for reporting the measured and forecasted erythemally effective UV irradiance. The implementation of UVI in different monitoring networks requires a globally, harmonized calibration scale. A paper on the harmonization of UVI measurements has recently been published [*Johnsen et al. 2008*].

Arrangements of radiometer intercomparisons have proved to be a practical way to establish a common reference scale and to validate and improve the worldwide agreement in measurement results. In these arrangements, a collection of radiometers representing national UV monitoring networks are synchronized and co-located with a group of high-quality reference spectroradiometers, traceable to international standards. For broadband meters, several international intercomparisons have been conducted [*Leszczynski et al., 1995; Bais et al., 2001b*], which have greatly improved the accuracy and comparability of measurements with these radiometers. For MBFRs there are still relatively few publications documenting the accuracy and performance in network applications. Up to 2005 there have been no international intercomparisons dedicated to this type of radiometers.

The following report includes results from the first international intercomparison of MBFRs. Forty-three radiometers participated, representing measurement sites and networks from Antarctica to the Artic, North and South America, Africa, Nepal and Europe. An overview of measurement sites interlinked with MBFRs participating in the intercomparison is given in Annex A2. The intercomparison had two major tasks: The first includes characterization of the radiometers' spectral and angular response functions in order to convert the raw detector outputs to spectral irradiance at standard wavelengths in the UV, with accuracy comparable to high-resolution spectroradiometers. The characterization work enabled the generation of look-up tables for total ozone and cloud optical depth, as well as irradiance calibration functions for alternative biological action spectra [*Dahlback, 1996*]. This information becomes available to the users. The second task includes a blind intercomparison of the UVI provided by the participants against the spectroradiometer reference, based on the participants' own data processing tools and their own or manufacturer's calibration. Finally, a set of new calibration functions is constructed, harmonizing UVI measurements from MBFRs with the spectroradiometer reference. The harmonized results are compared with the participants' own results.

2. SETUP AND METHODS

In order to ensure objectivity in measurement results, the campaign was accomplished according to established practices for blind intercomparisons [*Kjeldstad et al., 1997*]. Participants visiting the Norwegian Radiation Protection Authority (NRPA) during the core-period installed their own radiometers. Participants that were only shipping the radiometers had people from NRPA to do the set up. A spectroradiometer intercomparison of four instruments was run during the core-week. The purpose of this spectroradiometer intercomparison was to investigate the agreement in spectral calibration scales and to establish a set of reference spectra for the MBFR intercomparison. The agreement in spectroradiometer scales were analyzed from blind measurements at the end of the core-period. This preliminary analysis was done by CMS. The raw data collected from the MBFRs was processed by their owners. Results of the UV index measurements were not made available before the deadline for data submission.

2.1 Location and conditions

The intercomparison and laboratory work took place at Østerås, a semi-rural district 10 km north-west of Oslo. The campaign core-period, when most radiometers were operating (33 MBFRs), lasted from late April to mid-June 2005. The first three weeks were allocated to laboratory work and the weeks thereafter to solar measurements. After the end of the core-period, most radiometers were shipped back to their home institutions. Six new MBFRs were operating in the period from 24'th to 29'th June and four new MBFRs were operating in the period 16'th September to 10'th October. One of the MBFRs participating in the core-period served as transfer standard in these periods, because the reference spectroradiometer was not operating after the core-period. All radiometers were mounted at a uniform height of 2.50 m above the platform's base and oriented with their reference markers pointing in the north direction. The platform is located on the roof of the building of NRPA (59.946°N, 10.598°E, 145 m asl). The photo in Figure 1 shows the collection of radiometers present during the core-period. A flattened fish-eye photo (Figure 2), taken at the centre of the platform's reference plane revealed a sky view factor of 98.8% relative to a flat horizon. The photo shows that the sky view is uniform. For this period of year, the maximum solar elevation is 51.7° (SZA 38.3°). Observations during the core-period showed that there were no significant shadows from nearby trees or buildings along the sun's trajectory. During the measurement campaign the daily mean total ozone amount measured at the University of Oslo

Figure 1. **Solar platform at the roof of NRPA during the core period of the intercomparison. Front section: Eppley TUVR and Solar Light broadband meters flanked by two rotating shadowband MBFRs. Right section: NILU-UVs, GUVs and the front optics of 4 Bentham spectroradiometers. In the background and to the far right: Davis automated weather stations. (*Photo: G. Janson, USDA).***

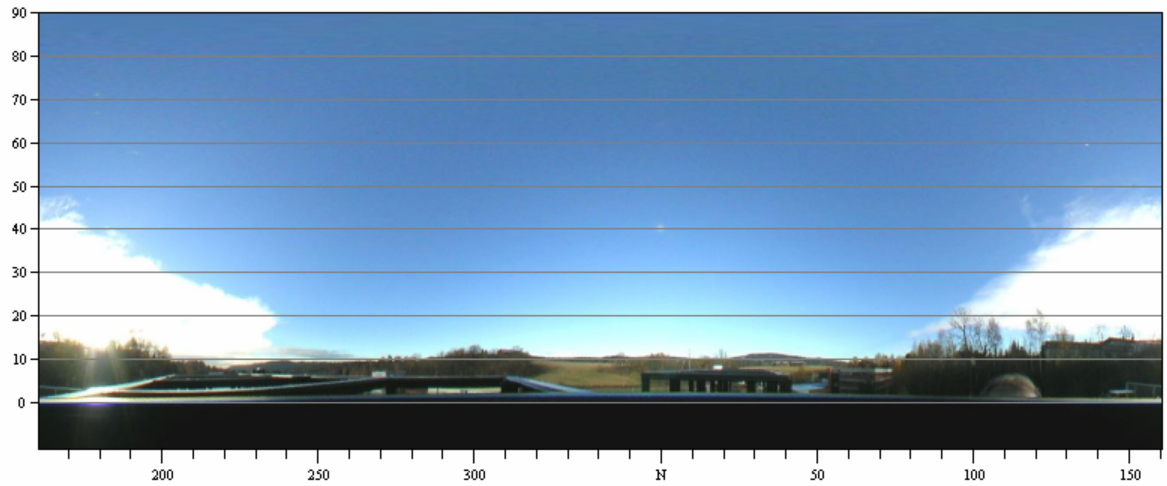

Figure 2. **Flattened fish-eye photo of the sky, as viewed in the radiometer's reference plane. Sun elevation (y-axis), azimuthal direction (x-axis), with azimuth 0 corresponding to North. The quartz dome of the front optic of a spectroradiometer is seen in azimuth 110. Effective sky view 98.8 percent of an unobstructed horizon.**

varied between 320 and 400 Dobson Units (DU). This is quite typical for the site and time of the year. The weather was highly unstable (Annex A1). Rainfall and fog frequently occurred, with periods of clear sky and broken cloud cover. All radiometer heads were cleaned at sunrise and immediately after the cessation of the rain in order to avoid impurities and droplets to interfere with the measurements. During the core-period, only May 27 (day of year 147) offered clear sky and stable conditions for most of the day.

2.2 Instrumentation

Three kinds of UV radiometers took part in the intercomparison: High-resolution spectroradiometers with approximately 0.5 nm to 1.0 nm bandwidths at full width half maximum (FWHM), multiband filter radiometers with spectral bandwidths 2 to 10 nm and a limited number of erythemal broadband meters. The broadband meter comparison was not officially part of the campaign, and the results are thus not published here.

2.2.1 Multiband filter radiometers

MBFRs from three manufacturers were represented in the intercomparison: The GUV Ground-based UV radiometers (16 in total) from Biospherical Instruments Inc. [*http://www.biospherical.com/*], the NILU-UV radiometers (25 in total) from NILU Products AS [*http://www.nilu.no*] and the UVMFR-7 multifilter rotating shadowband radiometer (MFRSR, 2 in total) from Yankee Environmental Systems Inc. [*http://www.yesinc.com/*]. A brief presentation of models, number of detector channels, nominal centre wavelengths and bandwidths (FWHM) is provided in Table 1. The names of participants representing different instrument types are given in Annex A2. All models have temperature stabilized detector heads and simultaneously record global horizontal irradiance at five to seven wavelengths. The MFRSRs also measure diffuse irradiance, using a shadow band. This allows calculation of direct irradiance from consecutively measured global and diffuse sky irradiances. Accurate synchronization of measurements is crucial when the sky conditions are unstable and the averaging period is within a few seconds. In the present campaign we managed to keep almost all measurements synchronized within ±2 s. The NILU-UVs and GUVs were continually recording irradiances with respectively 1 s and 10 s averaging periods. The MFRSRs recorded global and diffuse sky irradiances every 20 s, with a few seconds averaging periods. More information on GUVs, NILU-UVs and MFRSRs operating in UV-monitoring networks may be found in the works by *Bernhard et al. [2005]; Johnsen et al. [2002]; Aalerud et al. [2005], Høiskar et al. [2003]; Lakkala et al. [2005]; Gelsior [2004], and Bigelow et al. [1998]; Min and Harrison [1998]; Davis and Slusser [2005]*.

Among the 39 MBFRs participating in May and June and the four additional MBFRs participating in late September, UVI data from 25 radiometers were submitted by the participants. One of the participants provided a second data set for his radiometer, based on an alternative set of calibration factors. Eleven of these 26 data sets have independent calibration scales (GUV 9273 from Norway, GUV 9297 from UK, GUV 4121 from Sweden, GUV 4123V from USA, GUV 29233 from Nepal, MFRSR 00286 from USA, NILU-UV 4102 from Finland, NILU-UV 4106 from Greece, NILU-UV 990304 from Belgium, NILU-UV 990310 from Spain and NILU-UV 990319 from Poland).

The remaining 15 UVI series, representing two or more MBFRs from each networks, have interlinked calibration scales. Hence, one should keep in mind that these 15 data sets were not fully blind. Among them, 11 correspond to GUVs operating in the Norwegian UV monitoring network (GUV serial numbers 9222, 9270, 9271, 9272, 9274, 9275, 9276, 29222, 29229, 29237, 29243), one correspond to a GUV from USA (GUV 4123S), one correspond to one of the MFRSRs from USDA (MFRSR 00292), and two correspond to NILU-UVs from Spain (NILU-UV 990339) and Finland (NILU-UV 990331).

The remaining 18 radiometers (25-43), where no UVI results were provided by the participants, are NILU-UVs that operate or are planned to be operating in the Antarctic, Africa, Tibet and Nepal, or serve as transfer standards for other radiometers.

Table 1. **Types and number of MBFRs, for which the participants provided their own, processed UVI. Total number of MBFRs of each type is given in paranthesis in column 5. The extra 305-channel in one of the GUV-2511's is indicated in paranthesis in column 3.**

Radiometer type	Number of channels	Nominal centre wavelengths, nm	FWHM, nm	Number of MBFRs submitting UVI	Manu-facturer
NILU-UV I[a]	6	305, 312, 320, 340, 380, PAR (400-700)	10	5 (12)	NILU[b]
NILU-UV II[c]	6	305, 312, 320, 340, 380, PAR (400-700)	10	2 (14)	NILU[b]
GUV-511	5	305, 320, 340, 380, PAR (400-700)	10	1 (1)	BSI[d]
GUV-541	5	305, 312, 320, 340, 380	10	13 (13)	BSI[d]
GUV-2511	7 (8)	305, (305), 313, 320, 340, 380, 395, PAR (400-700)	10	2 (2)	BSI[d]
MFRSR	7	300, 305, 311, 317, 325, 332, 368	2	2 (2)	YES[e]

[a]With large diffuser

[b]NILU Products AS

[c]With small diffuser

[d]Biospherical Instruments Inc.

[e]Yankee Environmental Systems Inc.

2.2.2 Spectroradiometers

Three Bentham DM150 spectroradiometers and one Bentham DTM300 took part in the intercomparison. The Austrian company CMS Ing. Dr Schreder GmbH, with assistance from Innsbruck Medical University, operated the university's DM150. This radiometer has demonstrated high accuracy in several earlier European intercomparisons on broadband meters and spectroradiometers [*Leszczynski et al., 1995; Kjeldstad et al., 1997; Bais et al., 2001a, b*]. One DM150 was operated by the Norwegian University of Science and Technology (NTNU) and NRPA operated a DM150 and a DTM300 spectroradiometer. All operators and the three DM150s have been participating in the EC project Quality Assurance of Spectral Ultraviolet Measurements in Europe [see, eg., *Bais et al., 2001b*, and *http://lap.physics.auth.gr/qasume/*]. The monochromators and electronics were operating within temperature stabilized boxes, applying fibre optic light guides for solar radiation input. Two of the spectroradiometers utilized temperature stabilized front optics, purged with a small flow of clean nitrogen gas to keep humidity away. All spectroradiometers applied input optics with very good angular response in the UV. Global sky cosine errors were in the order of a couple of percent in the UV. All spectroradiometers made scans from 290 nm to 410 nm. The DTM300 additionally scanned up to 800 nm, in order to cover the photosynthetic active wavelength region (PAR). The cosine errors in the PAR are significant for the spectroradiometers from NRPA, thus numerical corrections were applied for both radiometers, assuming clear sky conditions for all scan moments. Errors in wavelength scales were corrected by the users and spectra deconvoluted to 1.00 nm bandwidths (FWHM), applying the shicRIVM software package [*Slaper et al., 1995*]. The DM150s were scheduled to make UV scans every 10 minutes after start at 04:00 UTC, with a fixed sampling rate of 2 s per 0.5 nm. The DTM300 was running with adaptive scan speed, independent on the scan schedule of the other spectroradiometers. Spectral measurements from the four spectroradiometers were converted to UVI according to the description given in *WHO [2002]*.

2.3 Selection of reference

A set of reference data may be selected on the basis of a single radiometer or the mean or median of spectra for selected radiometers. The use of a single instrument is easiest, as there will be the same reference for all the campaign period. The disadvantage is that systematic errors and

anomalies in a single reference will be transferred to other radiometers. A group reference will be less dominated by systematic errors than a single instrument. However, the calibration scale may not be consistent for the whole period, as there may not be the same group of radiometers in the reference all the time. The period all radiometers are operating concurrently may also be too short for the calibrations, or may not overlap for the period of most favourable conditions.

In order to decide which method is most suitable for the campaign we made a comparison of spectral scans and UVI for the four day period all spectroradiometers were operating (day of year 143-146). A comparison of UV spectra indicated agreement within ±4% for the NRPA and CMS150 spectroradiometers for the wavelength range 305 nm to 390 nm [*Johnsen et al., 2006*]. The agreement with NTN150 was within -10%, gradually improving to -5% at the end of the campaign period. However, unfavourable weather conditions and small synchronization errors resulted in spectral ratios that were too scattered to reveal any diurnal variability. Instead, we chose to compare the diurnal variability in UVI measured with the spectroradiometers and one of the MBFRs (GUV29222) on day of year 144. This day had periods with sunshine and cloudy conditions, which is evident from the upper panel in Figure 3, showing UVI recorded by five radiometers as a function of time. The graphs indicate that the four spectroradiometers closely matched the dynamic nature of rapid sampling with the GUV. The next two panels show the ratios in UVI versus time and SZA, relative to the UVI of spectroradiometer NRP150. NRP150 was selected as denominator for this illustration because it was operating throughout the full the core-period, with the same scan schedule as NTN150 and CMS150. All ratios were within approximately ±10% for most of the day. Selecting the spectroradiometers belonging to CMS and NRPA and the multiband filter radiometer GUV29222, the agreement in UVI scales were within ±5% for SZA less than 75°. Compared with the uncertainty range estimated for state of the art spectroradiometers [*Bernhard and Seckmeyer, 1999*] and the results from the latest successful spectroradiometer intercomparisons [*Bais et al., 2001b; Paulsson and Wester, 2006*], the results were consistent with what may be expected from first-class measurements.

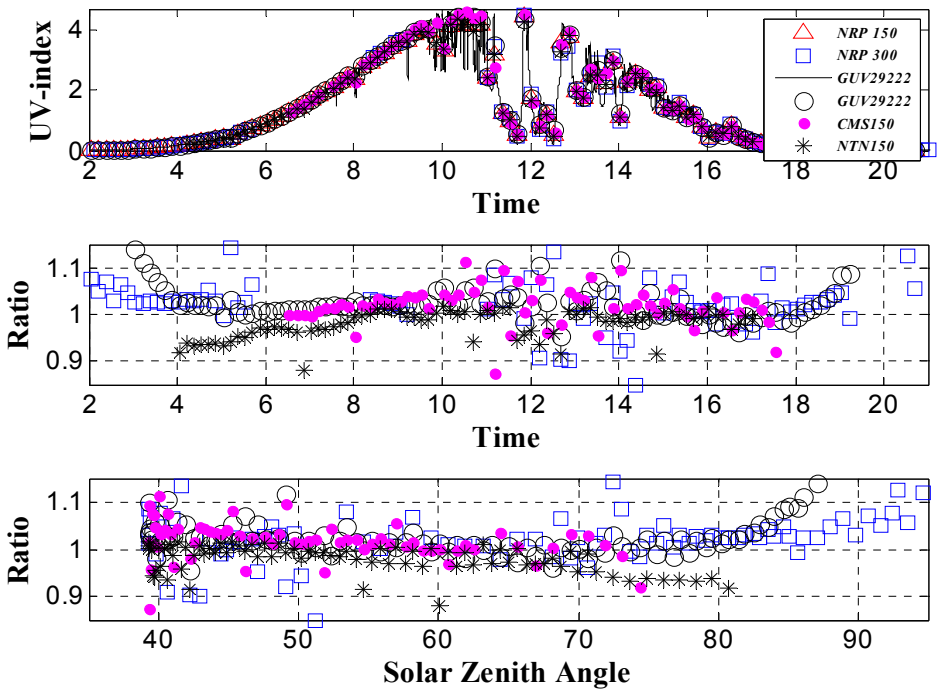

Figure 3. **UV-index measured by four spectroradiometers (NRP150 (triangle), NRP300 (square), CMS150 (filled circle) and NTN150 (star)), and continuous measurements with GUV 29222 (opern circle and solid curve), as a function of time. Ratio of UV index relative to NRP150 as function of time and solar zenith angle on day of year 144 2005.**

The spectroradiometers NRP150 and NRP300 continued operating until day of year 160, when periods of more favourable weather conditions occurred than in the spectroradiometer comparison period. Clear sky conditions at noon on day of year 147 enabled comparison with a radiative transfer (RT) simulated UV spectrum, using total ozone (325DU) and surface albedo (5%) as input parameters. The RT-model applied was the LibRadtran version 1.1-beta software package for radiative transfer calculations [*Mayer and Kylling, 2005*]. Ratios of measured and modelled spectra, smoothed with a running average of ±2.5 nm, were within ±4% from unity for the wavelength range 295 nm to 400 nm, with a mean difference of 2 - 4% between the two spectroradiometers [*Johnsen et al., 2006*]. Diurnal discrepancies in spectra of the NRP150 [*Meinander et al., 2006*], which were not evident for the DTM300, made the latter spectroradiometer be the natural choice. This spectroradiometer formed the basis for comparisons performed in the core-period. The comparisons of UVI performed in the second and third period were based on the GUV29222, which served as transfer standard.

2.4 UVI from MBFRs

The Global UV index [*WHO, 2002*] is defined as (Eq. 1)

$$\mathrm{UVI} = 40\int_{\lambda} \mathrm{W_{CIE}}(\lambda)\mathrm{E}(\lambda)\mathrm{d}\lambda \qquad (1)$$

W_{CIE} is the CIE erythemal action spectrum for Caucasian skin type [*McKinlay and Diffey, 1987; ISO, 1999*] and E_λ is the spectral horizontal irradiance in units of W/m^2nm. According to *Dahlback [1996]*, biologically effective irradiance from measurements with a MBFR may be approximated as a linear combination of outputs from UV channels (Eq. 2).

$$[1+\varepsilon(\Omega,\theta)]\cdot\sum_i a_i U_i = \sum_j W(\lambda_j)E(\lambda_j)\cdot\Delta\lambda_j \qquad (2)$$

U_i is the net current of detector channel i, a_i is the coefficient of the linear combination, j is a wavelength index, ε is a residual correction function, with input parameters total ozone amount Ω and solar zenith angle θ. The participants processed UVI results from their own radiometers, applying their own implementation of the Dahlback-method and either their own calibration or that provided by the radiometers' manufacturer. Literature references for the methods applied by the participants and the radiometer serial numbers are given in Annex A3.

2.5 Harmonization of UVI scales

The harmonized UVI scale is defined as a set of coefficients a_i and correction function ε in Eq. 2 determined such that the difference with the campaign's reference is minimal. The set of linear equations may in principle be solved with an analytical or an empirical approach. The analytical approach is based on RT simulated clear sky spectra and spectral characterizations of the detector channels' responsivity functions [*Dahlback, 1996*]. In the present work, the harmonization of UVI is based on the empirical approach, regressing real sky spectral measurements with detector outputs for the whole period the MBFR and the reference radiometer were operating (Eq. 3)

$$\varepsilon(\theta)\cdot\sum_i a_{i,\mathrm{CIE}}\cdot(U_{ik}-U_{ik}{}^0)/\mathrm{DF_i}(\mathrm{day},\mathrm{day}^0) \approx \sum_j W_{\mathrm{CIE}}(\lambda_j)E(\lambda_{jk})\cdot\Delta\lambda_j \qquad (3)$$

where $a_{i,CIE}$ are coefficients for calculating erythemally weighed irradiance, (U_{ik} - $U_{ik}{}^0$) is the net detector output of channel i matching in time the k'th measured spectrum E, $DF_i(day,day^0)$ are correction factors accounting for drift in responsivity relative to day of year day^0 = 147, and ε is a correction function that is dependent on SZA. The correction ε(θ) is required because a linear combination of a limited number of detector channels does not sufficiently capture the SZA-dependence of the UVI. There will be some uncertainty because ε(θ) is derived from data measured during clear and overcast skies without distinguishing of sky conditions.

The different timing of samples U_{ik} and E_{jk} were accounted for, using the method explained in section 2.8. The determination of drift $DF_i(day,day^0)$ is determined by the regression of daily mean absolute spectral responsivity with the corresponding day number, where the absolute spectral responsivity is defined in section 2.6.1.

The system of equations (Eq. 3) was solved in two steps. In the first step, ε(θ) was initially set to unity and $a_{i,CIE}$ were determined by multi-linear regression. A subset of U_{ik} and E_k was selected from the total period where MBFRs and the reference were overlapping in time, with additionally constrains of SZA ≤ 90°, total ozone amount between 250 DU and 500 DU, and UVA cloud optical depth (CLOD) either smaller than 5, 10 or 50, depending on signal-to-noise ratios for the actual MBFR. The use of a subset of data resulted in more robust sets of coefficients $a_{i,CIE,}$ compared to using all samples overlapping in time. The correction function ε(θ) was determined next, as a polynomial fit, using the $a_{i,CIE}$ from above. Conversion from CIE-effective irradiance to UVI is given in Eq. 4

$$a_{i,UVI} = 40 \cdot a_{i,CIE} \tag{4}$$

2.6 Laboratory characterizations

Laboratory characterizations of spectral and angular response functions are fundamental for most calibration purposes. Characterizations enable simulation of the detector output as function of e.g. SZA, the construction of calibration functions and the construction of a wide range of data products, including UVI. During the campaign period the relative spectral responsivity functions were measured for all detector channels. Angular response functions were measured for all GUVs, both MFRSRs and a selection of NILU-UVs. Absolute calibrations with 1000 W quartz tungsten halogen lamps (QTH) were made for Norwegian GUVs only, as part of the quality assurance procedures for the network operation. An overview of all laboratory characterisation work is shown in Annex A4.

2.6.1 Spectral responsivity function

The peak-normalized spectral responsivity r_i of detector channel i at wavelength λ_k is implicitly given in Eq. 5

$$U_{ik} - U_{ik}^{\,0} = K_i \int_{\lambda_j} \Phi(\lambda_k, \lambda_j) r_i(\lambda_k) d\lambda \tag{5}$$

The left side corresponds to the net detector output of detector channel i, and the right side to the integration of the vector product of r_i and the flux distribution Φ of a narrow bandwidth excitation source, tuned for wavelength k and with a distribution across wavelengths $\pm\lambda_j$. K_i is a constant equal to the absolute spectral responsivity at the wavelength of maximum response. K_i may be established from concurrent outdoor, global sky measurements with the MBFR and a reference spectroradiometer (Eq. 6), using the peak-normalized responsivity function r_i determined from laboratory measurements

$$K_i = \frac{(U_i - U_i^{\,0}) \cdot GCCF(\varphi_0, \theta_0, \lambda_0)}{\sum_j E(\lambda_j) \cdot r_i(\lambda_j) \cdot \Delta\lambda_j} \tag{6}$$

where GCCF is the global sky cosine correction function at wavelength λ_0, SZA θ_0 and azimuth angle φ_0, defined in section 2.7, and $E(\lambda_j)$ is the spectral irradiance corresponding to wavelength j for a given scan.

The characterization of r_i was based on a laboratory set-up, consisting of a wavelength-tuneable and narrow bandwidth excitation source, optics for imaging the excitation beam onto the detectors, a calibrated reference photo detector, measuring the flux of the excitation beam, and

electronics for data acquisition and control. The source consisted of a 1000 W Xenon arc lamp, mounted in a lamp housing (Oriel model 66021), and double monochromators (Oriel MS-257, model 77700). The lamp output was stabilized, using a light-intensity controller system (Oriel model 68850) that provided optical feedback to the power supply. A condenser lens, a focussing lens and heat absorbing water filter input radiation to the slit of the first monochromator. The wavelength scales of the monochromators were calibrated using a low pressure mercury lamp inserted in the pathway between the input slit and the Xenon lamp.

The beam passing the exit slit of the second monochromator was collected with a large concave mirror and distributed as uniformly as practicably achievable over the front optic of the reference detector and MBFR under test. The mirror was mounted on a computer controlled rotation stage, enabling alternating excitation of the reference detector and MBFR for each wavelength setting of the monochromators. The reference detector was a Si photodiode from United Detector Technology (model 222AUV), calibrated at the SP Technical Research Institute of Sweden in 2002. The detector dark signals were measured for each wavelength setting, using the internal shutter in the first monochromator, and subtracted from the total signals. In this way, possible drift in the net output of the test and reference radiometers could be accounted for. The spectral responsivities for NILU-UVs and GUVs were measured for the wavelength range 270-410 nm, with 1.0 nm increments, using slit widths corresponding to bandwidths of respectively 1.6 nm and 4.0 nm (FWHM). Measurements were also made for the PAR region for some of the radiometers that have a detector channel in the visible. The spectral bandwidths of the detector channels in the MFRSRs were very small compared with the other MBFRs. In order to accomplish high resolution measurements for MFRSRs, the wavelength increment of the excitation source was set to 0.1nm, using slit widths corresponding to 0.5 nm, 0.8 nm, 1.6 nm and 4.0 nm band widths. The responsivity functions resulting from scans with different bandwidth settings were approximated as (Eq. 7)

$$r_i(\lambda_k) \approx \frac{U_{ik} - U_{ik}^{\,0}}{\Delta\lambda \sum_j \Phi(\lambda_k, \lambda_j)} \tag{7}$$

From this set of r_i's a trial solution was assembled, constructing the central region of r_i from measurements with the smallest bandwidth and dynamic range, while the more distant parts and wings were obtained from measurements with wider bandwidths and dynamic range. The trial solution was next tested against clear sky spectroradiometer scans, and modified until the set of K_i in Eq. 6, corresponding to one value for each measured solar spectrum, were acceptable constant (±2%) for SZA less than 75°. See Annex A5 for a detailed description of the method.

2.6.2 Angular response function

The relative angular response C_i of a detector channel i is defined as (Eq. 8)

$$C_i(\varphi_0, \theta_0, \lambda_k) = \frac{U_i(\varphi_0, \theta_0, \lambda_k) - U_i^{\,0}}{\cos(\theta_0) \cdot \max(U_i - U_i^{\,0})} \tag{8}$$

where U_i-U_i^0 is the net signal induced by a uniform, collimated beam of radiation at wavelength λ_k, striking the detector at θ_0 angle of incidence and φ_0 azimuth angle. The set-up for characterizing the angular response consisted of a 150 W Xe-lamp (Oriel 66002) with a collimating lens, a stack of WG305 cut-off filters to mimic a typical noon solar spectrum, a horizontal rotation stage and baffles between the source and rotation stage. The radiometer was positioned with the surface of the input optic at the axis of rotation. The angle between the optical axis of the set-up and the axis of the input optic corresponded to the SZA, and the azimuth angle φ_0 was defined by the rotation about the axis of the input optic. A 3D mapping of the angular response was performed for azimuth intervals of 45° or 90° and zenith angles from 0° to 90°, with variable step intervals. Signals U_i^0 induced by dark current and scattered radiation were measured for every angular setting, using a shutter to temporally block the input beam.

The lens collimator was adjusted in order to obtain a visually uniform field, overfilling the surface of the radiometer input optic, and still have acceptable signal-to-noise ratio at very high high θ_0. Due to the off-axis positioning of detector elements, any small inhomogeneities in the input beam may result in an apparent azimuthal cosine response. This pitfall was discovered at a later stage, when most cosine characterizations had been completed. By repeating the characterizations for a few radiometers, with the collimator adjusted to get a much more uniform field for the cost of reduced signal-to-noise ratio, the influence from inhomogeneities could be estimated. For radiometers with small diffusers (GUV 9273), the first inhomogenous beam measurements of cosine responses agreed within -4 % to 2 % for each azimuth orientation and $\theta_0 \leq 80°$, which justified the first method of adjusting the collimator. However, this was not appropriate for the series of NILU-UV radiometers with the largest diffusers. Repeated characterizations for NILU-UV 990319 showed that the original, inhomogenous beam measurements differed by up to 15 % for some azimuth directions and $\theta_0 \leq 80°$ for those detector channels that were off-axis mounted. The concentrically mounted 305-channel showed much more consistent results; within 0 to 4 % for the same range of angles. Due to this finding, the homogenous beam results for the 990319 were applied as template for all NILU-UVs with big diffusers. For the later version of NILU-UVs with small diffusers, only 3 radiometers were characterized; two for inhomogenous beam and one (NILU-UV 4118) for homogenous beam. Assuming identical cosine response for all of them and comparing inhomogenous beam results with the results for 4118, differences by 0 to 13 % were seen for some azimuth orientations and $\theta_0 \leq 80°$. By the same argumentation, cosine results for the NILU-UV 4118 were applied as template for all NILU-UVs with small diffusers.

Final results of cosine characterizations are shown as 3D polar plots in Figure 4 for one of the GUVs, measured with a homogenous beam (GUV 9273). In this example the angular responses drop continuously from 1.00 at SZA 0° to a minimum of 0.65 at 90°. Skew circles in the 3D plots indicate some azimuthal variations in the angular responses, which were apparent for most MBFRs. Azimuthal variations is better seen when plotted as function of SZA (Figure 5). In this example the azimuthally mean responses are fairly similar for all detector channels. However, some azimuthal differences are seen: The 306 nm and 340 nm channels display smallest variations and the 315 nm and 320 nm channels the largest variations, with differences of ±1% and ±4% at 80°, respectively. An implication of this is that global sky measurement results may not be consistent unless the radiometers are set up with a fixed azimuthal orientation.

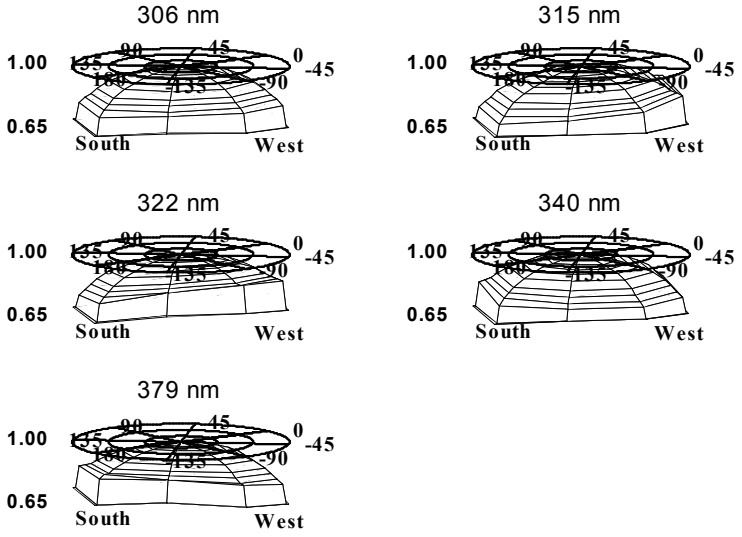

Figure 4. 3D polar plot of the relative cosine responsivity of instrument GUV 9273 for five UV channels, as function of solar zenith angle (30, 60 and 90 given as circles on the top) - and azimuth angle (given in intervals of 45 degrees). Direction 0 defines sun in the azimuthal North direction.

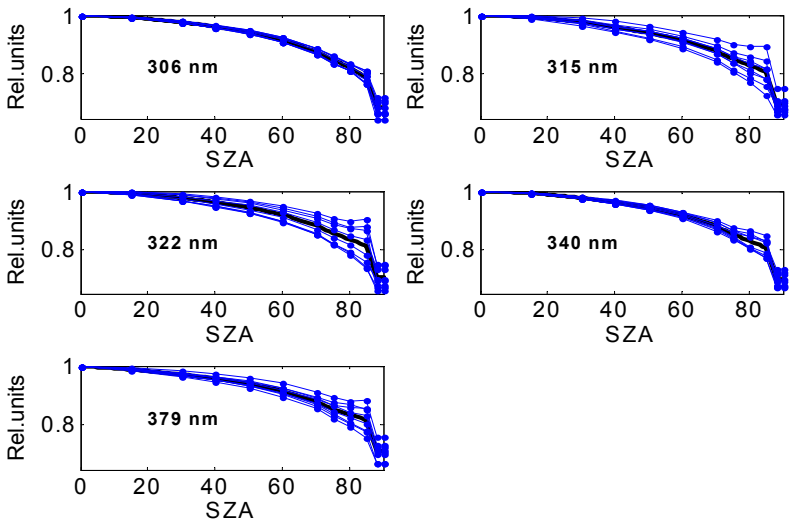

Figure 5. **Relative cosine responsivity of instrument GUV 9273 for five UV channels as a function of solar zenith angle. The solid curve represents an average for all azimuthal directions and closed circles represent specific azimuth given in intervals of 45 degree.**

2.7 Global sky cosine correction function, GCCF

Non-perfect angular responses lead to errors in measurements of global spectral irradiance. The errors may be corrected by multiplying raw irradiance measurements with the Global Sky Cosine Correction Function (GCCF). GCCF is the reciprocal of the Global Cosine Ratio (1/GCR) (Eq. 9), defined as the ratio of global spectral irradiance E^*_{actual}, simulated for the actual sky radiance distribution and the angular response of the radiometer, and the global spectral irradiance E_{ideal} resulting from substituting the actual angular response with the ideal cosine response [*Seckmeyer and Bernhard, 1993*].

$$GCCF_{i,Clearsky}(\varphi_0,\theta_0,\lambda_k) = \frac{1}{GCR_i(\varphi_0,\theta_0,\lambda_k)} = \frac{E^*_{i,glob,ideal}}{E_{i,glob,actual}} \tag{9}$$

For diffuse sky conditions, the UV hemispherical sky radiance distribution may be approximated as isotropic. GCR simplifies to the diffuse sky cosine ratio CD_i (Eq. 10)

$$GCR_{i,Diffuse}(\lambda_k) = CDi(\lambda_k) = \frac{E^*_{i,actual}}{E^*_{i,ideal}} = 2\int_0^{\pi/2} \overline{C_i}(\theta_0,\lambda_k)\cdot\cos(\theta)\sin(\theta)d(\theta) \tag{10}$$

where $\overline{C_i}$ is the azimuthally averaged angular response for SZA θ. For clear sky conditions, GCR is approximated as a weighted sum of the direct horizontal irradiance E_{dir}, diffuse irradiance E_{dif} and global irradiance E_{glob} (Eq.11)

$$GCR_{i,Clearsky}(\varphi_0,\theta_0,\lambda_k) = \frac{E_{dif}(\lambda_k)}{E_{glob}(\lambda_k)}\cdot CD_i(\lambda_k) + \frac{E_{dir}(\lambda_k)}{E_{glob}(\lambda_k)}\cdot Ci(\varphi_0,\theta_0,\lambda_k) \tag{11}$$

The GCCFs calculated with Eq. 9 were applied only for the determination of the absolute spectral responsivity factors K_i. Other calibrations have been based on empirical fitting functions ε, that implicitly include the effects of cosine errors, errors in the determination of r_i, non-linearity in detector responses etc. For the period day 142 to152, GCCFs for wavelengths up to 368 nm were based on measurements of the direct/diffuse and diffuse/global irradiance ratios from the rotating

shadow band radiometer MFRSR s/no 00286. For wavelengths above 368nm, spectral ratios were based on model simulations for clear sky and partly cloudy cases, flagging cloudy sky conditions from the diffuse/global ratio measurements of the 368 nm channel. For the rest of the campaign period, the ratios were based on clear sky model simulations only.

2.8 Matching of different time bases

The spectroradiometer chosen as reference utilized intensity-adapted scan speeds, with durations of scans lasting from 160 to 190s for the whole core-period and SZA less than 90 degrees. MBFRs operating during the core-period utilized fixed sampling speeds, recording radiation at frequencies of 0.05 Hz to 3 Hz and averaging periods of 1 second for NILU-UVs, and 10 or 60 seconds for GUVs. In order to compare measurements from MBFRs with the measurements from the scanning spectroradiometer, the time base of MBFR measurements needs to be matched with the spectroradiometer time base. Otherwise, perturbations resulting from variable sky conditions become unequally reflected in the two measurement series, resulting in excessive scatter in ratios of the two measurement series.

In order to match different time bases, the following method was chosen: Scan periods overlapping with the time scale of MBFRs were first selected, before interpolating the detector outputs to the sampling times corresponding to the respective spectroradiometer scans $E(\lambda_{jk})$. The effective time stamps $T_{eff,k}$ of response-weighted or CIE-weighted spectrum k was calculated with Equation 12:

$$T_{eff,k} = \frac{\sum_j t_{jk} W(\lambda_{jk}) E(\lambda_{jk}) \Delta T_{jk}}{\sum_j W(\lambda_{jk}) E(\lambda_{jk}) \Delta T_{jk}} \quad (12)$$

where t_{jk} is the time when wavelength λ_j in spectrum k is measured, ΔT_{jk} is the time step of each wavelength step and W correspond to respectively the CIE erythema action spectrum or relative spectral response of each detector channel. The effective detector outputs $U_{ik,}$ corresponding to each spectrum and detector channel i (Eq. 3) were calculated as a weighted mean of the interpolated detector outputs U_{ijk} (Equation 13):

$$U_{ik} = \frac{\sum_j U_{ijk} W(\lambda_{jk}) E(\lambda_{jk}) \Delta T_{jk}}{\sum_j W(\lambda_{jk}) E(\lambda_{jk}) \Delta T_{jk}} \quad (13)$$

2.9 Conversion of raw data to units of spectral irradiance

The detector output of MBFR channels represents a response-weighted average of irradiance over a wavelength region that is typically significantly wider than the bandwidth of a high-resolution spectroradiometer. During the course of a day, the variations in spectral shape in solar spectra induce shifts in the effective wavelength regions recorded by the MBFR. This results in SZA dependent mismatch between the raw output of MBFR channels and the spectral irradiance recorded at fixed wavelengths by a spectroradiometer. Hence, a correction function is needed in order to convert detector outputs from MBFRs to measurements representing spectral irradiance at fixed wavelengths. The radiometer erythemal calibration equation of a broadband meter [*Webb et al., 2006*] serves this purpose (Eq.14)

$$E_i(\lambda_{nom})[W/m^2 nm] = C_i \cdot (U_i - U_i^0) \cdot F_{mat,i}(\lambda_{nom}, \Omega, \theta) \cdot \varepsilon(\theta, CLOD) \quad (14)$$

where E_i is the spectral irradiance of the reference, corresponding to bandwidth 1.00 nm (FWHM), C_i is a calibration factor for detector channel i, $(U_i\text{-}U_i^0)$ is the net detector output, F_{mat} is a conversion function depending on wavelength λ, total ozone Ω and SZA θ, and ε is one of two SZA

dependent correction functions, defined for small and high cloud optical depths (CLOD), respectively. The nominal wavelengths λ_i were selected from a set of centre wavelengths, typical for MBFRs (Table 2).

Table 2. Nominal wavelength of detector channels of GUV, NILU-UV and MFRSR, for which the spectral calibration functions have been established.

GUV:	305 nm,	313 nm,	320 nm,	340 nm,	380 nm,	(395 nm, 560 nm)
NILU-UV:	305 nm,	313 nm,	320 nm,	340 nm,	380 nm,	560 nm
MFRSR:	300 nm,	305 nm,	311 nm,	317 nm,	325 nm,	332 nm, 368 nm

The spectral conversion function $F_{mat,i}$ is given as (Eq. 15)

$$F_{mat,i}(\lambda,\Omega,\theta) = \frac{\sum_j W_{i,j} E_j(\Omega,\theta)}{\sum_j r_{i,j} E_j(\Omega,\theta)} \quad (15)$$

where E_j is RT-modelled spectral irradiance at wavelength λ_j and given SZA and total ozone, $r_{i,j}$ is the relative spectral responsivity of radiometer detector channel i at λ_j. $W_{i,j}$ is unity at the nominal wavelength of detector channel i and zero else. The function was normalized to SZA 40° and total ozone amount 300 DU. Eq. 14 was solved in two steps, initially solving C_i for SZA < 70° and ε set to unity. Total ozone amount was taken from daily observations with a Brewer spectroradiometer, located at the University of Oslo. In the second step, ε was determined as a polynomial fit between the left and right side of Eq. 14, selecting observations corresponding to CLOD < 1.5 and CLOD > 1.5. CLOD was based on the detector channel corresponding to wavelengths between 360 nm and 380 nm, using a look-up table for the conversion of detector output and corresponding SZA, and CLOD [*Dahlback, 1996*]. Finally, C_i was updated after the application of ε(CLOD<1.5) and ε(CLOD>1.5).

3. RESULTS

3.1 Comparison of UVI provided by the participants

Comparison of UV Indexes processed by the participants, relative to the spectroradiometer reference, revealed distinct differences in total mean values and standard deviations for the core period and SZA ≤ 80° (Figure 6, red symbols). A group of 12 MBFRs showed remarkable close agreement (GUV serial numbers 9222 to 29243). These radiometers operate in the same UV network in Norway. Their calibration scales rely on the same transfer standard, in contrast to the results for most other participating MBFRs, which applied independent calibration scales and processing tools for calculating UVI. Hence, a larger variability is expected for data sets created independently from the other. Selecting independent data sets only, corresponding to one MBFR for each user group, 11 data sets are left. Out of these 11 sets, 8 (73%) were within ±5%, while 10 (90%) were within ±10% from unity. Including all radiometers providing UVI (25 MBFRs and 26 data sets), the mean values for 20 sets (75%) were within ±5% from unity and 23 data sets (88%) were within ±10%. Considering that the weather conditions were highly variable during the campaign period, the agreement within ±5% for more than 70% of the data sets is surprisingly good. The results were markedly better than those achieved in earlier intercomparisons of erythemal broadband meters, where deviations of ±20% or more were revealed [*Leszczynski et al., 1995; Bais et al., 2001b*]. One of the latest successful international spectroradiometer intercomparisons [Bais et al., 2001a] showed that 11 out of 19 instruments (60%) from all around the world agreed within ±5% from the reference. The European intercomparison NOGIC2000 [*Paulsson and Wester, 2006*] showed similar results; 7 out of 10 (70%) spectroradiometer-derived sets of UVI agreed within ±5%. Compared with this, the MBFR results exhibited a similar degree of

consistency, although spectroradiometers represent the currently most accurate instrumentation for measuring UVI.

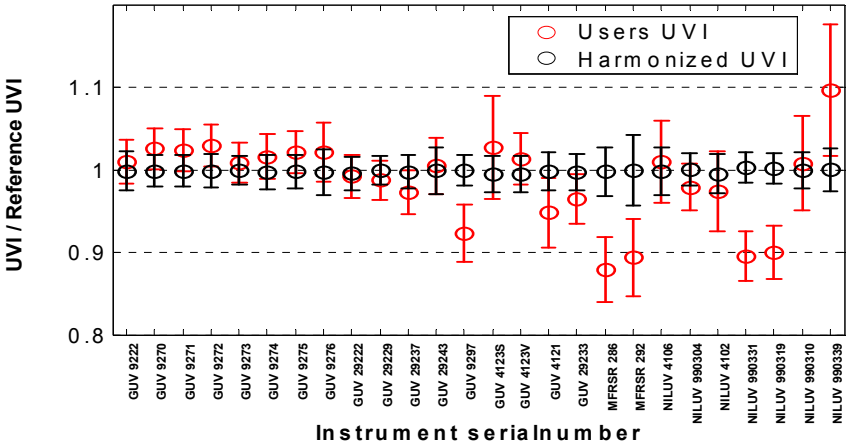

Figure 6. **Mean ratios of participant's UVI and the reference (red circles) and harmonized UVI and the reference (black circles) for 25 MBFRs operating in the core period. X-axis: Instrument serial number. Y-axis: Relative units. Error bars indicate ±1σ, for SZA<80°. Reference in period is NRP300.**

3.2 Harmonized UVI results

The harmonization of UVI obtained by regressing MBFR raw data against the reference spectra (Eq. 3) resulted in markedly closer agreement than any of the participants' data sets (Figure 6). The ratios for the entire core period are plotted as a function of SZA in Figure 7. Either group of collective data are centred around unity (zero deviation from reference), but the harmonized ratios display markedly less scatter (±4.6% (±2 σ) for SZA ≤ 80°) than the participants' ratios (±11.6%), as well as significantly smaller divergences from unity at high SZAs. Analysis of harmonized UVI results for all 33 MBFRs operating in the core period, showed similar good agreement for all types of MBFRs (Figure 8). The collective ratios are well within ±5% for all sky conditions, even for SZAs close to 90°. Comparing participants' data and harmonized data, the improved agreement for large SZAs (> 70°) is due to the fact that the harmonized results utilized the SZA dependent correction function epsilon ε in Eq. 3, whereas results from participants were based on ε set to unity for all SZAs. Results for individual MBFRs are shown in Annex A6.

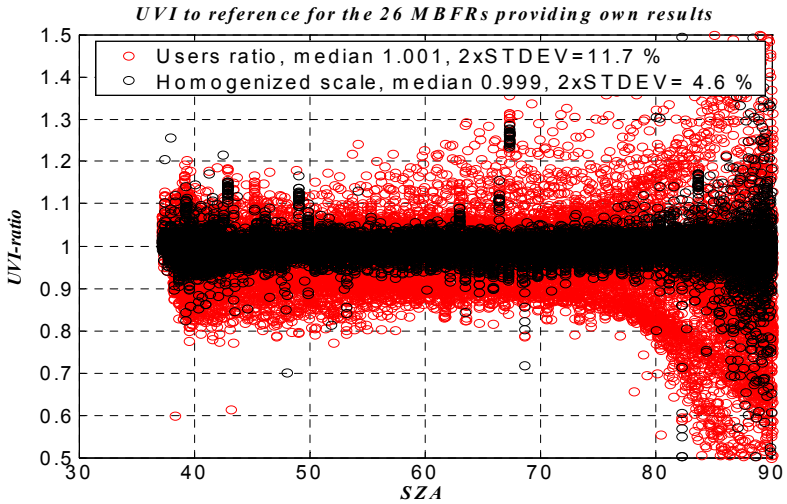

Figure 7. **Ratio of participant's UVI from 25 MBFRs to the reference NRP300 (red circles) for the campaign period 142 -160 as a function of SZA. 2σ is 11.7% for SZA< 80 degree. Ratios of harmonized UVI for 26 MBFRs to the reference NRP300 (black circles) for the same period. 2σ is 4.6% for SZA< 80 degree.**

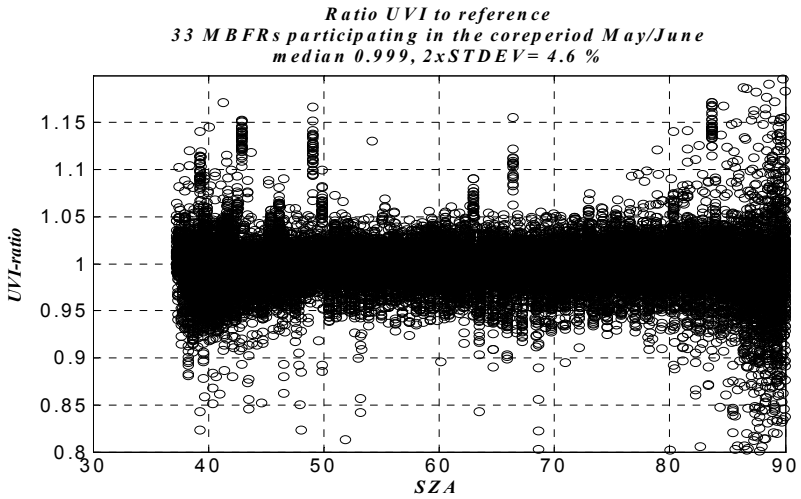

Figure 8. **Ratio of harmonized UVI to the reference for 33 MBFRs participating in the core-period day 142-160 in 2005, as function of solar zenith angle. 2σ is 4.6% for SZA < 80°. Reference in the period is NRP300.**

Six additional NILU-UVs, arriving in June and four NILU-UVs arriving in September/October were compared to the transfer GUV 29222, which had been calibrated against the reference previously. Harmonized UVI ratios for the two groups of radiometers showed median ratios close to unity (Figure 9 and Figure 10). The double standard deviations were larger for the six radiometers participating in the summer period (±6.5%) than for the four radiometers participating in the autumn period (±4.6%), and show some azimuthal discrepancies, which are less evident in the last period. This might be related to differences in the angular response functions for the transfer standard GUV 29222 and NILU-UVs, and the dominating sky conditions for the two periods. The summer period had mostly clear sky conditions whereas the autumn period had mostly overcast conditions. Thus, any azimuthal discrepancies in angular responses would be more evident in the first period. The results were based on the transfer standard instead of the spectroradiometer reference, which implies that the uncertainties in harmonized UVI are expected to be larger than for the core period.

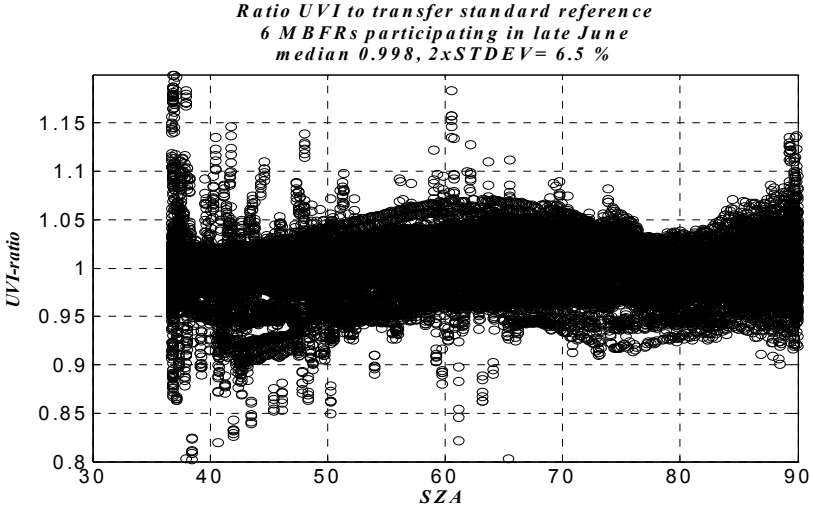

Figure 9. **Ratio of harmonized UVI to the reference for six MBFRs participating in the period day 170-180 in 2005, as function of solar zenith angle. 2σ is 6.5 % for SZA<80 degree. Reference in period 170-180 is GUV 29222.**

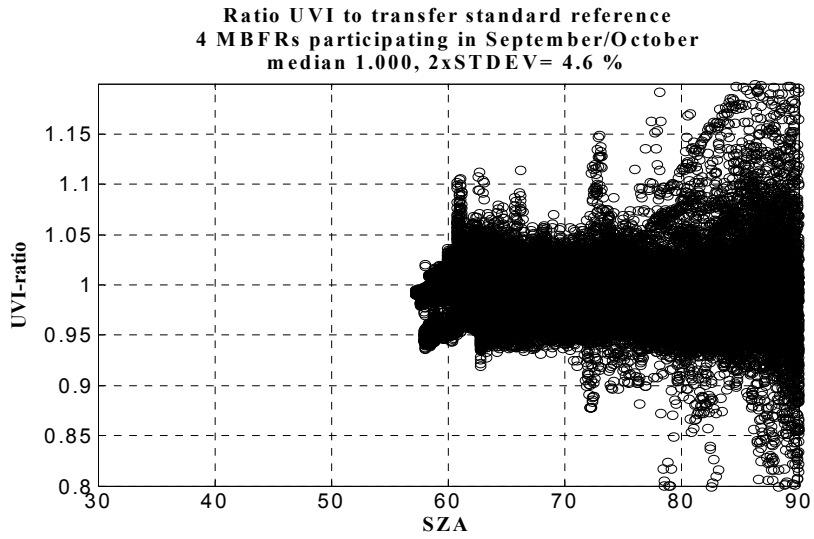

Figure 10. **Ratio of harmonized UVI to the reference for four MBFRs participating in the period day 260-280 in 2005, as function of solar zenith angle. 2σ is 4.6 % for SZA<80 degree. Reference in period 260-280 is GUV29222.**

Cumulative distributions of participants' UVI ratios versus the absolute differences from unity for SZAs less than respectively 50°, 60°, 70°, 80° and 90° (Figure 11) show similar distribution patterns for all SZAs except 90°. More than 80% of the participants' ratios deviate less than ±10% from unity for SZA ≤ 80°, and 95% are within ±12% for SZAs ≤ 90°. Harmonized UVI ratios reveal identical distribution patterns for all SZA intervals. More than 95% of all samples deviate less than ±5%, which is almost a factor 3 closer to the reference than the participants' data. Histograms of the relative number of ratios deviating within a relative difference in ±x percent from the reference (inserted figure) display a sharply centred Gaussian-looking distribution of harmonized ratios, whereas ratios calculated from data provided by the participants have a relatively wide bimodal distribution. The bimodal distribution results from the fact that the majority of participants' UVI had slightly higher values than the reference, whereas a small group of MBFRs also displayed significantly lower values.

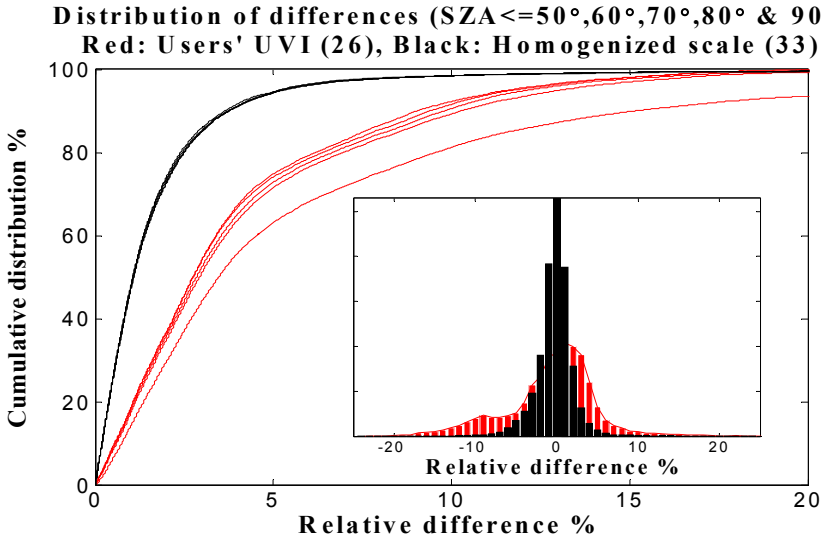

Figure 11. **Cumulative distribution of participant's UVI values (red curves) and harmonized UVI values (black curves) deviating up to ±20% from the reference UVI. Five curves represent SZAs < 50°, < 60°, < 70°, < 80° and < 90°. Same data shown as histogram in inserted figure. Red is participant's data and black is harmonized data.**

3.3 Factors influencing the quality of UVI data

The intercomparison of UVI from participants (Figure 6, Figure 7 and Figure 11) indicated significant differences in the calibration scales and standard deviations for some radiometers. Deviations from the reference of up to 12% were seen, with standard deviations ranging from ±2% to ±8% for SZA < 80°. Deviations and uncertainties in measurement results may be related to differences in the methodology for retrieving UVI from raw measurements and influences from different environmental conditions, or instrument-related discrepancies and effects from differences in operational procedures at the home and the campaign location. The influence from these uncertainty sources is discussed in the next sections.

3.3.1 Uncertainties related to the methods of UVI retrieval

The results of user-data and harmonized data were all based on linear combinations of detector outputs, with different choices of coefficients $a_{i,CIE}$, and correction functions epsilon ε in Eq. 2 and Eq. 3. The values in ε were close to unity for SZA less than about 70°. Hence, differences in standard deviations of retrieved UVI values must be related to the method in choosing optimal coefficients $a_{i,CIE.}$ Uncertainties related to the retrieval method were identified for three sets of participants' data, representing UVI ratios for GUV 4123 (two data sets labelled GUV 4123V and GUV 4123S) and NILU-UV 990330 (Figure 12). The first two data sets (left and middle panel) correspond to the same radiometer, but display different degrees of scatter, related to different choices of coefficients and combinations of detector channels. The scatter is most prominent for NILU-UV 990339 (right panel). This participant also submitted UVI for another radiometer (NILU-UV 990310), but with significantly less scatter. The participant informed that the two NILU-UVs were calibrated on different dates, locations and sky conditions. The influences from different sky conditions and locations will be discussed later in this section, but from what have been demonstrated above, the coefficient of linear combinations have a strong impact on the standard deviations.

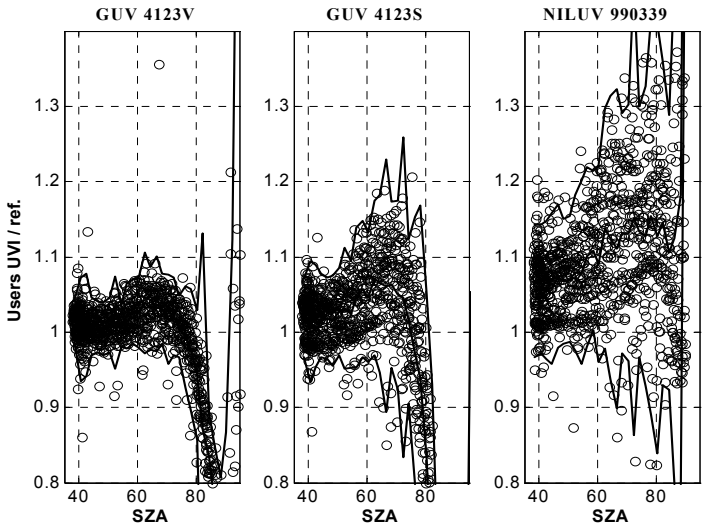

Figure 12. Ratio of UVI provided by owners of GUV 4123 and NILU-UV 990339 to the reference NRP300 for the campaign period 142-160, as a function of SZA. Left and mid panel show results for different choices of CIE coefficients and channels for GUV4123.

Some participants apply an analytical approach to solve the set of linear equations, based on detailed characterizations of the radiometer, RT-modelling and a comparison with a spectroradiometer. This method has the advantage that RT-simulations may take site-specific input parameters into account, optimizing data products for a certain location in the world. RT-simulations for realistic sky conditions other than clear sky are not trivial, which is neither the implementation of realistic corrections for radiometers displaying large cosine errors. During this campaign, a large set of measurements were acquired for almost all sky conditions. This facilitated

the use of an empirical approach to the harmonization of UVI. The method is solely based on observation data, i.e. responsivity functions and information on the cosine error are not required as they are inherent parts of the detector signals. Compared with the participants' ratios, the standard deviations for all groups of MBFRs are significantly smaller than any data sets provided by the participants (Figure 6 and Figure 7), and all ratios are close to unity. Differences in standard deviations may thus be related to the retrieval method, rather than indicating that one radiometer is performing well and another is not. Figure13 serves as illustration for this, showing remarkable less scatter in harmonized UVI after having reprocessed the raw data for the same radiometer.

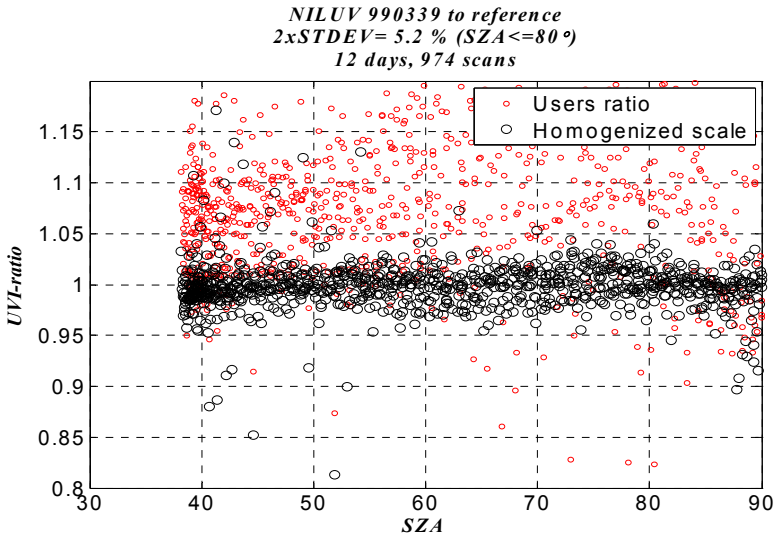

Figure 13. UVI provided by the owner of NILU-UV 990339 and harmonized UVI relative to the reference, as function of SZA for the campaign period 142-160.

3.3.2 Uncertainties related to different site conditions

Good agreement in harmonized results does not necessarily imply that the calibration functions are optimal for locations and conditions other than the campaign site. Among world wide locations, polar regions represent sky and surface conditions that are highly different from the semi-rural campaign site near Oslo. Surface albedo and SZA are very high for most of the year, with periods of extreme variations in the total ozone amount. In order to investigate the influences on UVI measurements from variable SZA, surface albedo, CLOD and total ozone, real sky and RT-simulated UVI-ratios have been examined.

RT-simulations for surface albedo 5% and 90% and SZA < 90° showed that the ratio of UVI from a typical MBFR and UVI from modelled spectra, applying (Eq. 3), differed only marginally (±0.1 % for SZA < 75° and ±0.3 % for SZA < 80°). . Hence, the calibrations are valid for all surface conditions from snowless to snow covered ground, as would also be the case for enhanced albedo from a dense cloud layer underneath the observation altitude.

Next, the influence on UVI ratios as a function of CLOD was studied, using real sky data and RT simulations. From the measurement data, no significant influences from varying CLOD were found for the prevailing sky conditions. RT-simulations showed that the effect is less than 1% for CLOD < 100 at all SZA, relative to clear sky conditions. For moderate and high SZA, the largest effect is found for SZA > 80° and CLOD > 500. The error contribution on an absolute level is however negligible as the UVI for CLOD > 500 is less than 2.5% of the clear sky value at SZA 80, which is beyond the detection level for most MBFRs.

Changes in total ozone affect the spectral shape of the solar spectrum. For the campaign period the daily mean total ozone varied between 320 DU and 400 DU. Analysis of UVI ratios did not indicate any systematic changes in ratios as function of total ozone for SZA 40° to 90°.

Dahlback [1996] has calculated that the deviations induced by variable ozone amounts are less than 5% for 200 - 500 DU and SZA < 80°. The largest deviations were found for combinations of small ozone amounts and small SZA and large ozone amounts and large SZA. UVI is very small for combinations of large SZA and ozone amounts. Dahlback included an ozone correction term (Eq. 2), whereas our empirical approach (Eq. 3) did not. With exception of very low ozone amounts combined with small SZA, the correction term is within a few percent from unity, which for most conditions is well within the uncertainty of the reference spectroradiometer. Recalling that the campaign results showed close agreement in harmonized UVI for a wide range of weather conditions, SZA and moderate ozone amounts, one might expect that the empirical, harmonized calibration functions are valid for most cases and sites, with exception of combinations of very small ozone amounts (< 200 DU) and small SZAs. Hence, good consistency in harmonized UVI may be expected for a wide range of SZA, CLOD and surface conditions. This makes MBFRs particularly useful for UV monitoring.

3.3.3 Calibration and instrument related uncertainties

In addition to the influences from different methodology in UVI retrieval, the scatter in the participants' UVI ratios could also be attributed to differences in calibration scales (Figure 6). One group provided UVI data that were significantly lower (-11 to -13%) than the mean of the collective data set. The group reported that this finding was consistent with preliminary results from an intercomparison arranged in 2003. The group had recently received new calibration coefficients from their calibration supplier, which effectively enhance the UVI reported for the clearest days by +12%. If the new calibration coefficients had been applied, the results would shown much closer agreement with those of the other participants.

Most data sets showed consistent UVI ratios for the campaign period. However, a few data sets indicated daily increases by more than 0.5% in the mean UVI ratios for the period the radiometers were operating [*Johnsen, et al., 2006*]. This effect may not have been fully accounted for by the participants, as the quantification of drift in instrument responsivity functions would require comparison with a stable campaign reference prior to the data submission. This effect was accounted for in the processing of harmonized UVI (Figure 7). Two of the groups reported that they had noted a significant increase in the absolute responsivity for their MBFRs, while these radiometers otherwise performed stable at the home locations. A plausible explanation for this may be the use of different solvents and routine cleaning intervals for the operation at the campaign site and the home locations. During the intercomparison period, the front optics were cleaned every morning with Isopropanol Prima. This solvent is recommended by one of the MBFR manufacturers. MBFRs participating in the campaign had all flat diffusers without any protective quartz dome, which makes the front optic of MBFRs more exposed to impurities and dirt accumulation than broadband radiometers protected by quartz domes. This applies particularly to those radiometers that have diffusers made of granular Teflon-like material, where impurities may be trapped inside. Impurities that may have slowly accumulated in the front optic material during normal operation may have become diluted from the use of more efficient solvents during the campaign period, resulting in enhanced UV transmittance towards the end of the campaign. In order to avoid step responsivity changes, which severely limit the value of intercomparison and harmonization of measurement results, the front optics should be maintained clean at the home location. This could be done either by applying a more efficient solvent and frequent cleaning intervals or installing a protective quartz dome above the diffuser. The installation of a protective quartz dome may, however, require re-characterization and re-calibration of the radiometer.

3.4 Relative spectral responsivity functions for each class of MBFRs

Spectral responsivity functions r_i were established from laboratory characterizations, and modified with empirical corrections based on the solar comparison with the spectroradiometer. The results for one radiometer from each category of MBFRs are shown in Figure 14 (GUV model 541 and 2511), Figure 15 (NILU-UV I and II, big and small diffuser) and Figure 16 (UV-MFRSR and NILU-UV II). As may be seen, the wavelengths at peak responsivity correspond fairly well with the nominal wavelengths (Table 2). The bandwidths (FWHM) are about the same (10 nm) and the slope of the cut-off towards higher wavelengths is fairly similar for the two GUV and the two NILU-UV models. The latest models (GUV-2511 and NILU-UV II) display slightly higher responsivity

towards the short wavelength cut-off. This has, however, minor significance for solar measurements, as the short-wave part of the band pass region adds only a small contribution to the total signal. The UV-MFRSRs display much narrower bandwidths (2 nm) and steeper slopes towards higher wavelengths than any GUV and NILU-UV. The position of centre wavelengths is also different from the other radiometers. Shoulders towards the higher wavelengths vary significantly among individual radiometers. Outdoor solar comparisons have shown that UVB channels with shoulders of magnitude10^{-4} or more have significance at moderate and high SZAs. Small errors in the laboratory quantification of the shoulders become critical for these radiometers, which require the use of empirical corrections to the r_i established from laboratory characterizations.

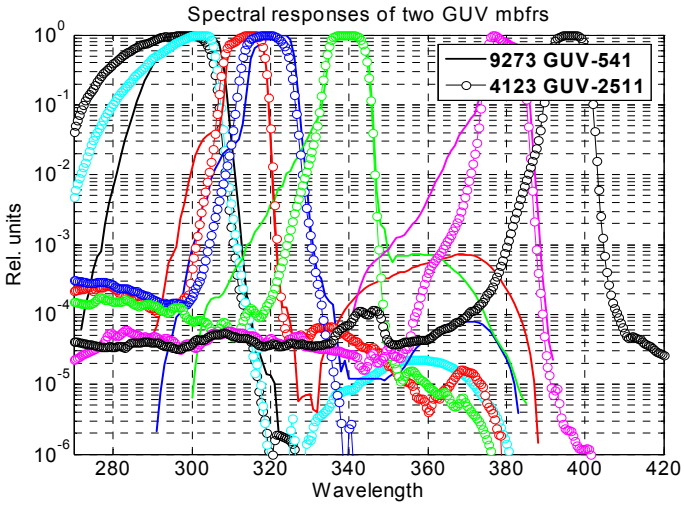

Figure 14. **Typical peak-normalized spectral responsivity of an early model GUV-541 (serial number 9273) and latest model GUV-2511 (serial number 4123) radiometer from Biospherical Instruments Inc. X-axis gives wavelength in nm. S/num 9273 (solid line) has five channels in the UV and serial number 4123 (circles) has seven channels in the UV.**

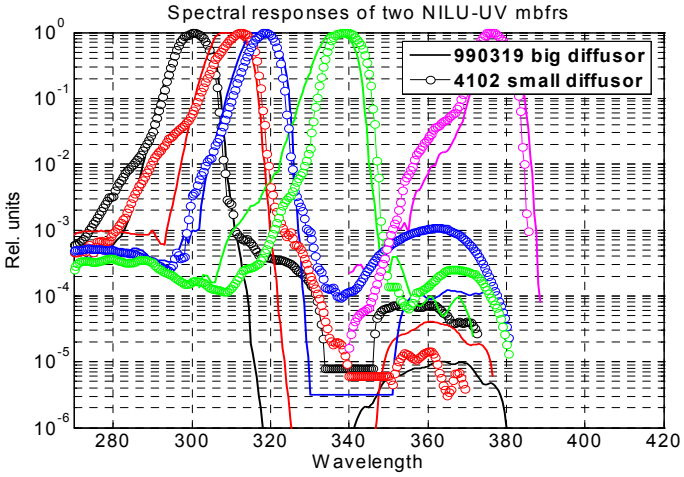

Figure 15. **Typical peak-normalized spectral responsivity of an early model NILU-UV I (serial number 990319, with big diffuser) and the latest model NILU-UV II (serial number 4102, with small diffuser) from NILU Products AS. X-axis gives wavelength in nm. S/num 990319 (solid line) and serial number 4102 (circles) have five channels in the UV and a PAR channel in the visible.**

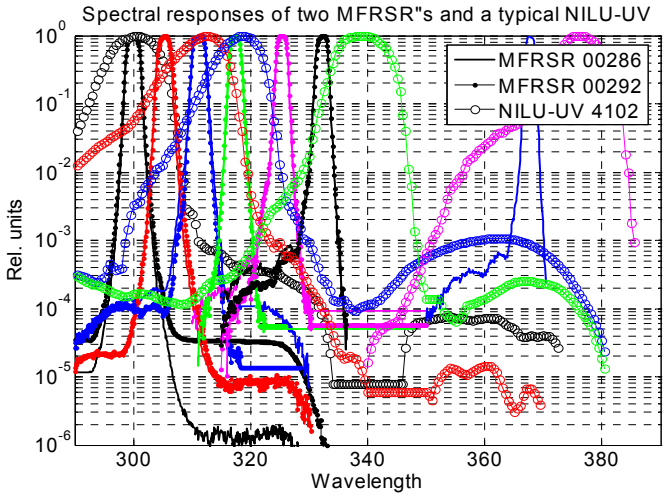

Figure 16. **Peak-normalized spectral responsivity of two UV-MFRSRs (solid lines) from Yankee Instruments Inc. and NILU-UV serial number 4102 (circles). X-axis gives wavelength in nm. The UV-MFRSRs have seven channels in the UV.**

3.5 Global cosine ratios (1/GCCF) for each class of MBFRs

Laboratory characterizations of the angular response functions and measurements of the global and diffuse sky irradiances enabled an evaluation of errors in global sky measurements for the different classes of MBFRs. Figures 17-21 show the global cosine ratio (GCR) for all detector channels (Eq. 11). The ratios are presented as a function of SZA, utilizing the 3D (red and green curves) and azimuthally mean (black line) angular response functions, respectively. Smooth irregularities indicate cloud effects, resulting from variations in the ratios of measured diffuse and global UV irradiances with the MFRSR. Step jumps, seen for channels above 368 nm, result from the use of the 368-channel of MFRSR as proxy for the sky conditions (clear, partly cloudy and fully overcast), combined with RT-simulated diffuse/global ratios for the three cases. GCR is equivalent to the reciprocal global cosine correction function (GCCF), and the cosine error in percent is equivalent with $100 \cdot (\mathrm{GCR}(\theta) - 1)$. More specifically:

- Figure 17 shows results as function of SZA for day of year 147 (mostly clear sky), for the five channels of GUV 9273, representing model GUV-541. GCR varies between 0.93 - 0.95 for channel 1 (305 nm), and 0.91 - 0.95 for channel 5 (380 nm). The azimuthal variation in GCR for rising and setting sun is 2%. Uncertainties from predictions of cloud-free and overcast conditions are up to 4%, with a maximum at 70° to 80° for the UVA channels.
- In Figure 18 the results are presented for GUV 4123, representing model GUV-2511. GCR is close to unity for channels 1 (305 nm)) to five (340 nm), and between 1.00 and 1.03 for channels six (380 nm) and seven (395 nm). Overlapping curves indicate that GCR is independent on the azimuth orientation. The largest deviations are seen for the PAR channel (channel 8), with GCR increasing from 0.99 (40°) to 1.08 (80°). The influence from shifting cloud conditions is 1 to 3% for the UV channels and 6% for the PAR channel. Compared with the early model GUV-541, the GCR corresponding to the new front optics have greatly improved.
- Figure 19 shows results for the NILU-UV model with the big diffuser (NILU-UV 990319). For small and moderate SZAs the GCR values are similar with GUV-541 (0.93), but drops to a deeper minimum of 0.90 to 0.85 at SZA 70° for the channel 1 and channel 5 (380 nm). The azimuthal effect is about the same as GUV-541 (2%), with slightly larger influences from shifting sky conditions (5% for channel 5). The largest SZA dependency is seen for the PAR channel (channel 6), with a minimum of 0.60 at SZA 80. The error resulting from uncertainties in the prediction of cloud-free and overcast conditions is up to 30% at SZA 80° for the PAR channel.

- Figure 20 applies to NILU-UV II with small diffuser (serial number 4102). GCR is 0.95- 0.97 for the five UV channels, with only small variations in SZA and almost no dependency on the azimuthal orientation, apart from the PAR channel (channel 6). Compared with the early model NILU-UV, the GCR corresponding to the new front optics have greatly improved.
- GCR corresponding to the UV-MFRSRs (Figure 21) is almost flat and close to unity for the seven UV channels. Compared with the other radiometer models, the angular responsivity is superior. The azimuthal dependency is in the order of 2%, similar with the GUV-541 and NILU-UV I.

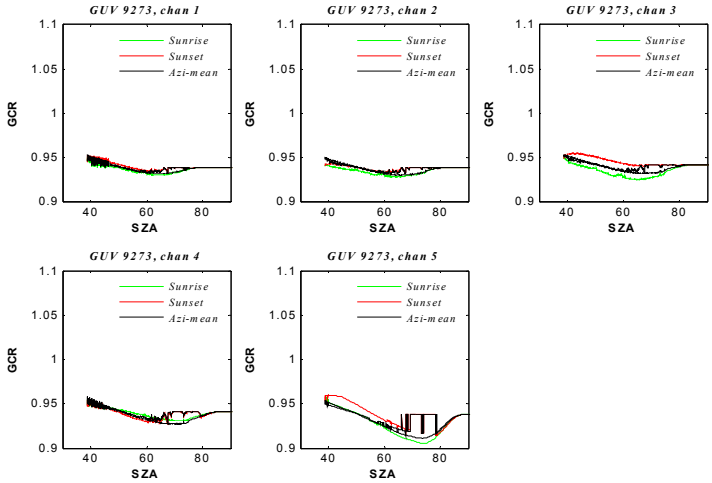

Figure 17. **Predicted reciprocal of global cosine correction function for instrument GUV 9273 (model GUV-541), as a function of solar zenith angle, for rising (green) and setting (red) sun. The correction function corresponding to azimuthally averaged cosine responsivity is indicated in black. Calculations are based on measurements of the horizontal direct and diffuse irradiance measured by a rotating shadow band MBFR on day of year 147 2005, and the angular responsivity functions established from laboratory characterizations.**

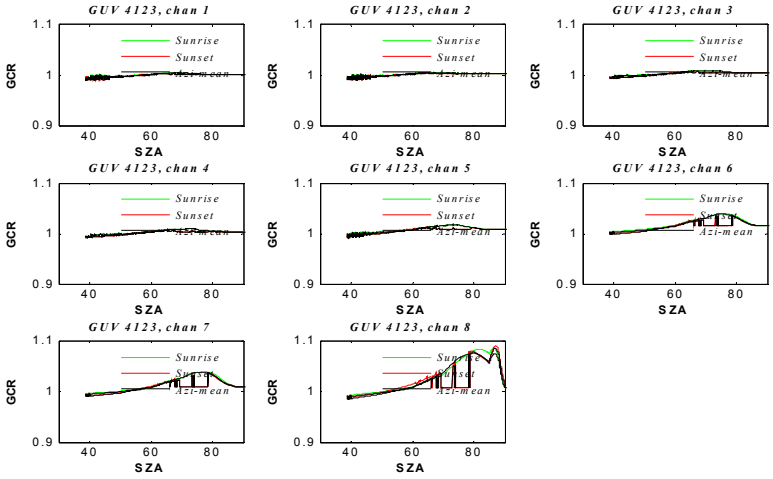

Figure 18. **Same as Figure 17, for GUV 4123 (model GUV-2511).**

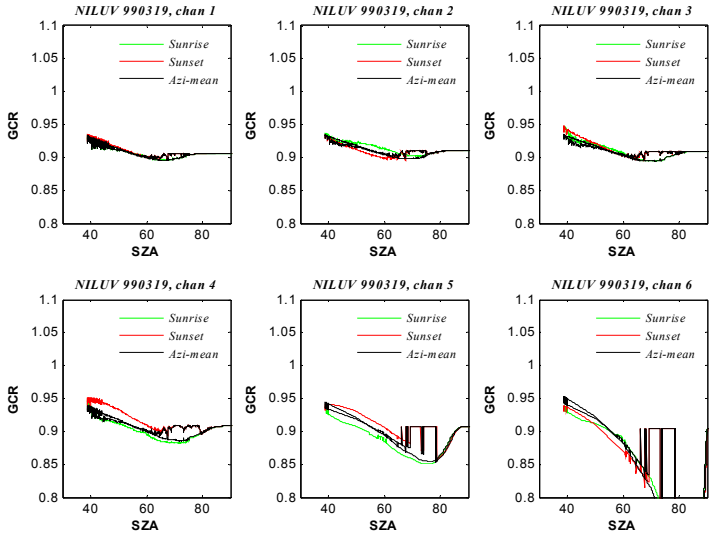

Figure 19. **Same as Figure 17, for NILU-UV 990319 (model NILU-UV I, big diffuser).**

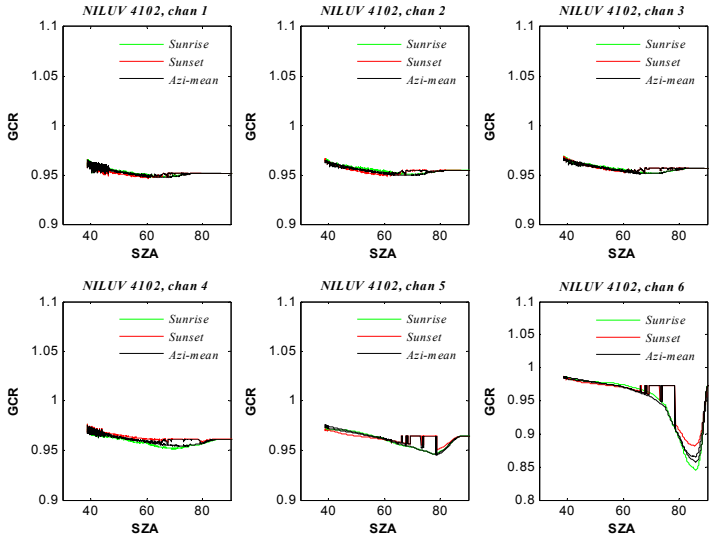

Figure 20. **Same as Figure 17, for NILU-UV 4102 (model NILU-UV II, small diffuser).**

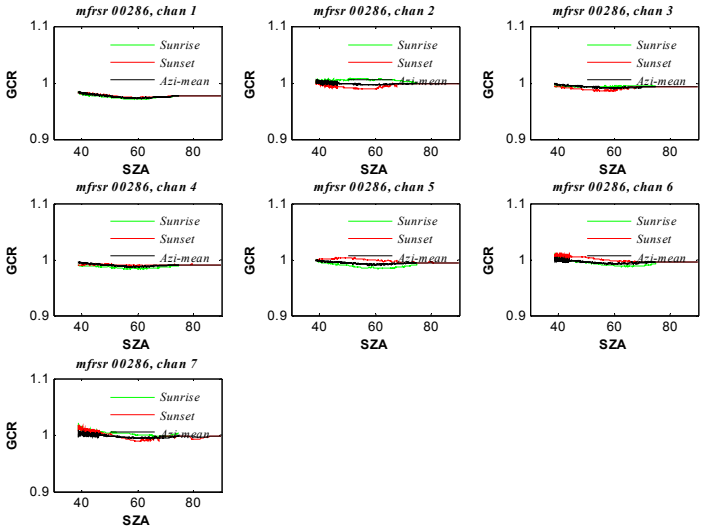

Figure 21. Same as Figure 17, for UV-MFRSR 00286.

3.6 Validation and Harmonization of spectral information from MBFR channels

3.6.1 Conversion of detector outputs to harmonized units of spectral irradiance

The output from detector channels may be converted to harmonized units of spectral irradiance, corresponding to measurements at fixed wavelengths with a high-resolution spectroradiometer (Eq. 14). The success of this method is demonstrated in Figure 22, showing ratios of respectively uncorrected (black) and corrected (red and blue) detector outputs from GUV 9273, relative to the spectroradiometer measurements. Each data point corresponds to scans performed during the core-period, plotted as function of SZA.

The uncorrected results of UVB channels display significant discrepancies for increasing SZA (20% to 40%), whereas UVA channels do not. Application of conversion functions F_{mat} and fitting functions ε result in flat, corrected ratios (red and blue circles) also for the UVB channels, only limited by scatter from low signal-to-noise ratios at high SZA. Hence, the corrected measurement results are proportional to the spectral irradiance measurements of a spectroradiometer. Standardization of measurement units for reporting detector outputs is desirable, because MBFRs and high-resolution spectroradiometers operating world wide get interlinked, despite differences in operation principles and detector characteristics.

The ratios, corresponding to the reciprocal calibration factor (1/C), vary between 80 and 100 for the five channels. These are reasonable values, as the radiometer detector outputs were originally calibrated by the manufacturer in units of $\mu W/cm^2/nm$ instead of $W/m^2/nm$, back in 1994 (conversion factor 100). Response changes resulting from ten year operation in the network were not accounted for prior to this analysis. This may partly explain the up to 20% difference in C based on the manufacturer's original calibration and the harmonized results.

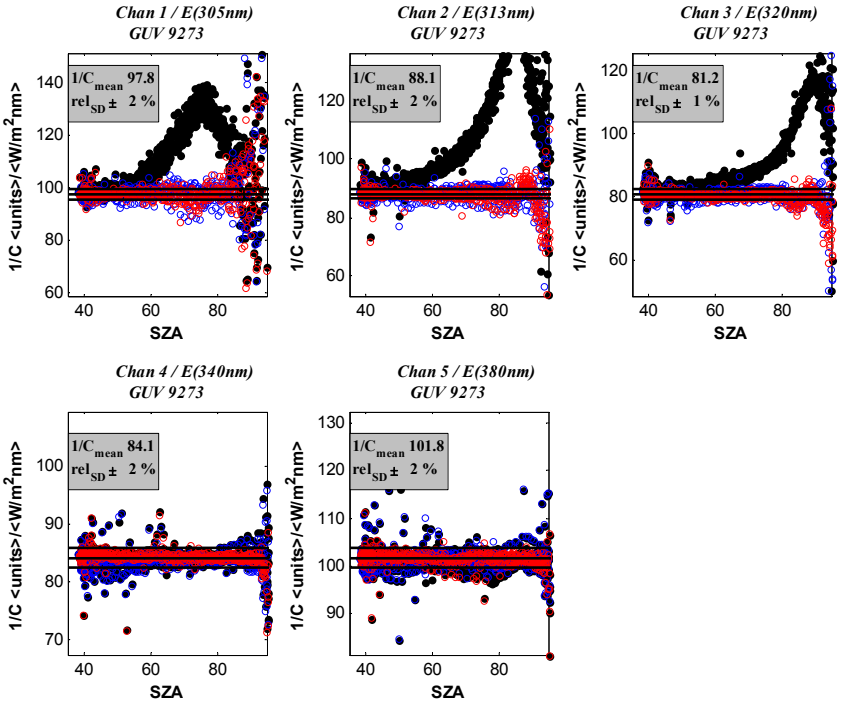

Figure 22. **Reciprocal calibration factor (1/C) for nominal centre wavelength of five channels of GUV 9273 as a function of SZA. Measurement unit is signal output/W/m^{2}nm. Black dots correspond to the ratio of MBFR output to the spectral irradiance of the reference. Blue and red dots correspond to ratios for rising and setting sun, utilizing the matrix correction method in Eq. 14. Perfect match with spectroradiometer corresponds to flat ratios.**

3.6.2 Fitting functions ε(SZA,CLOD) vs GCCF

The observed ratios $C_i \cdot (U_i - U_i^0) \cdot F_{mat,i}(\lambda_{nom}, \Omega, \theta) / E_i(\lambda_{nom})$, using C_i determined in the previous subsection, form the reciprocal correction function 1/ε in Eq. 14. In Figure 23 the ratios are shown as a function of SZA for rising and setting sun (blue and red circles). The ratios form two distinct groups, corresponding to clear sky cases (CLOD < 1.5, thin black line) and cloudy sky cases (CLOD > 1.5, thick black line). Ideally the ratios should reflect the reciprocal global cosine correction functions (1/GCCF) for the corresponding SZA and sky conditions. RT-simulated results for 1/GCCF and clear sky conditions (violet curve) are included in the figure for comparison with empirically determined clear sky observations of 1/ε. As may be seen the agreement in theoretical and empirical fitting functions is good for the two UVA channels, but distinct discrepancies are seen for the three UVB channels. This indicates significant errors in the spectral responsivity functions for the UVB region. Stray light, centre wavelengths and steepness of slopes are inevitably difficult to estimate and would be most significant for those detector channels measuring in the ozone cut-off region. However, as have been shown here, the application of fitting functions ε effectively removes most of the errors originating from errors in the spectral responsivity functions and possible non-linear detector responses.

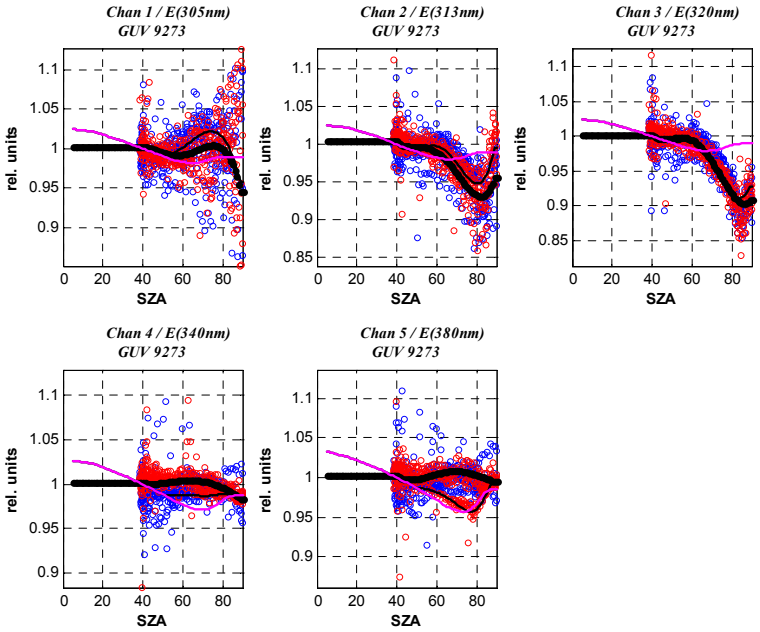

Figure 23. **Reciprocal fitting function (1 / ε(θ,CLOD)) in Eq. 14, which is applied as residual correction function for the convertion of detector output of GUV 9273 to units of spectral irradiance at standard wavelengths. Blue and red circles correspond to rising and setting sun. Thin black line is a polynomial fit where CLOD<1.5 and thick black line a polynomial fit where CLOD >1.5. Violet curve corresponds to the global cosine ratio GCR simulated for clear sky conditions.**

4. SUMMARY AND CONCLUSIONS

Scientific groups from all around the world were invited to take part in an intercomparison of multiband filter radiometers (MBFRs) in Oslo in 2005. Forty-three MBFRs joined the campaign, representing UV monitoring networks on most continents. Radiometers from three manufacturers were present; the GUV Ground-based UV radiometers from Biospherical Instruments Inc, the NILU-UV radiometers from NILU Products AS and the UVMFR-7 multifilter rotating shadowband radiometers from Yankee Environmental Systems Inc. The purpose was to assess and improve the comparability of measurements of Global UV Index (UVI) for all realistic sky conditions. The intercomparison was accomplished according to established practices for blind intercomparisons. A group of four high-accuracy spectroradiometers, three from Norway and one from Austria, served as basis for establishing a set of reference spectra for the comparison with UVI from participants. Twenty-six sets of UVI data were supplied by the participants. The mean ratios between participants' data and the reference were within ±5% for 20 data sets and ±10% for 23 data sets obtained during the core period and SZAs less than 80°. Excluding radiometers that were traceable to the same national calibration standards, 8 out of the remaining 11 sets of radiometer data were within ±5% and 10 out of 11 sets within ±10%. Harmonization of UVI resulted in close agreements with the reference, and the standard deviation for the collective group of 33 MBFRs operating in the same period was within ±4.6% (2 σ) for SZA up to 80°. Corresponding standard deviation for the collective group of 26 data sets from participants was ±11.7% (2 σ). The results show that the optimization of calibration coefficients and the use of a SZA-dependent correction function enable accurate measurements for a wide range of weather conditions, and likely also total ozone amounts and surface albedos. Hence, all types of MBFRs participating are highly useful for accurate measurements of UVI at high latitudes. Characterizations of spectral responsivity functions and angular responses enabled processing of total ozone amount and cloud optical depth for the radiometers. These input data were applied when each radiometers detector output were converted to units of spectral irradiance at standard, nominal wavelengths, corresponding to the bandwidth of a high resolution spectroradiometer (FWHM 1.00 nm). The harmonization of UVI and conversion of detector output to spectral irradiance at standard

wavelengths enable world-wide cross comparability of MBFRs operating in UV monitoring networks.

Acknowledgements

The intercomparison was supported by the World Meteorological Organization, The European Commission, through COST action 726, The Norwegian Research Council and The Norwegian Radiation Protection Authority, who hosted the campaign. The support made it possible to invite groups from all around the world to take part in this intercomparison, and to provide a link to several earlier European spectroradiometer and broadband meter intercomparisons. The arrangement is part of project 155810/720 Factors Controlling UV Radiation In Norway (FARIN), supported by The Norwegian Research Council.

References

Aalerud, T. N. and B. Johnsen (2006), The Norwegian UV-monitoring programme. Period 1995/96 to 2004, StrålevernRapport 2006:4. Østerås: Norwegian Radiation Protection Authority.

Bais, A., S. Topaloglou, S. Kazadzis, M. Blumthaler, J. Schreder, A. Schmalwieser, D. V. Henriques, and M. Janouch (2001a), The LAP/COST/WMO Intercomparison of Erythemal Radiometers. World Meteorological Organization (WMO). WMO/GAW Rep. 141.

Bais, A. F., B. G. Gardiner, H. Slaper, M. Blumthaler, G. Bernhard, R. McKenzie, A. R. Webb, G. Seckmeyer, B. Kjeldstad, T. Koskela, P. J. Kirsch, J. Gröbner, J. B. Kerr, S. Kazadzis, K. Leszcznski, D. Wardle, W. Josefsson, C. Brogniez, D. Gillotay, H. Reinen, P. Weihs, T. Svenoe, P. Eriksen, F. Kuik, A. Redondas (2001b), SUSPEN intercomparison of ultraviolet spectroradiometers, J. Geophys. Res., 106(D12), 12509-12526, 10.1029/2000JD900561.

Bernhard, G. B. and G. Seckmeyer (1999), Uncertainty of measurements of spectral solar UV irradiance, J. Geophys. Res., 104 (D12), 14321-14345.

Bernhard, G., C. R. Booth and J. C. Ehramjian (2005), Real-time ultraviolet and column ozone from multichannel ultraviolet radiometers deployed in the National Science Foundation's ultraviolet monitoring network, Opt. Eng. 44(4), 041011-1 - 041011-12.

Bigelow, S., J. R. Slusser, A. F. Beaubien and J. H. Gibson (1998),The USDA Ultraviolet Radiation Monitoring Programme, Bulletin of the American Meteorological Society, 601.

Dahlback, A. (1996), Measurements of biologically effective UV doses, total ozone abundances, and cloud effects with multichannel, moderate bandwidth filter radiometers, Appl. Opt. 35 (33), 6514-6521.

Davis, J. M. and J. R. Slusser (2005), New USDA UVB Synthetic Spectrum Algorithm. In Ultraviolet Ground- and Space-based measurements, Models, and Effects V, edited by Germar Bernhard, J. R. Slusser, J. R. Herman, and W. Gao, pp. 58860B-58860B-7, SPIE - The International Society for Optical Engineering, San Diego, CA, USA.

Gelsior, N. (2004), Studies on solar ultraviolet radiation and ozone over the Tibetan plateau, Ph. D. thesis, Univ. of Bergen, Norway.

Høiskar, B. A. K., R. Haugen, T. Danielsen, A. Kylling, K. Edvardsen, A. Dahlback, B. Johnsen, M. Blumthaler and J. Schreder (2003), Multichannel moderate-bandwidth filter radiometer for measuring ozone-column amount, cloud transmittance, and ultraviolet dose rates, Appl. Opt., 42, 3472-3479.

ISO (1999), Erythema reference action spectrum and standard erythema dose, International Organization for Standardization. ISO/CIE 17166.

Johnsen, B., O. Mikkelborg, M. Hannevik, L. T. Nilsen, G. Saxebøl and K. G. Blaasaas (2002), The Norwegian UV-monitoring programme. Period 1995/96 to 2001, Strålevern Rapport 2002:4. Østerås: Norwegian Radiation Protection Authority.

Johnsen, B., B. Kjeldstad, T. N. Aalerud, L. T. Nilsen, J. Schreder, M. Blumthaler, G. Bernhard, A. Bagheri, B. Bhattarai, C. Topaloglou, G. Zablocki, O. Meinander, B.A. Høiskar, R. Haugen, W.S. Durham, G. Janson, A.R. Marrero, A. Dahlback, D. Bolsée, J.R. Slusser, J. Stamnes, C. Torres, A.R.D. Smedley, L.-E. Paulsson, K. Lakkala, A.R. Webb, J.B. Ørbæk, A.A. Grimenes, T. Ringstad, T. Lange and W. Josefsson (2006), International intercomparison of multiband filter radiometers in Oslo 2005, Proc. of SPIE Vol. 6362, p. 63620W1-63620W12.

Johnsen, B., B. Kjeldstad, T. N. Aalerud, L. T. Nilsen, J. Schreder, M. Blumthaler, G. Bernhard, C. Topaloglou, O. Meinander, A. Bagheri, J. R. Slusser and J. Davis (2008), Intercomparison and harmonization of UV Index measurements from multiband filter radiometers, J. Geophys. Res., 113, D15206, doi:10.1029/2007JD009731.

Kjeldstad, B. Johnsen, and T. Koskela (eds.) (1997), The Nordic intercomparison of ultraviolet and total ozone instruments at Izaña, October 1996, Final report. Meteorol. Publ. 36, Finnish Meteorol, Inst., Helsinki.

Lakkala, K., A. Redondas, O. Meinander, C. Torres, T. Koskela, E. Cuevas, P. Taalas, A. Dahlback, G. Deferrari, K. Edvardsen, and H. Ochoa (2005), Quality assurance of the solar UV network in the Antarctic. J. Geophys. Res., 110.

Leszczynski, K., K. Jokela, L. Ylianttila, R. Visuri, and M. Blumthaler (1995), Report of the WMO/STUK intercomparison of erythemally-weighted solar UV radiometers. Spring/Summer 1995, Helsinki, Finland. World Meteorological Organization (WMO). WMO/GAW Rep. 112.

Mayer, B. and A. Kylling (2005), Technical note: The libRadtran software package for radiative transfer calculations – description and examples of use, Atmos. Chem. Phys. 5, 1855-1877.

McKinlay, A., and B. L. Diffey (1987), A reference action spectrum for ultraviolet induced erythema in human skin, in Human Exposure to Ultraviolet Radiation: Risks and Regulations, edited by W. Passchier and B. Bosnajokovich, Elsevier, New York.

Meinander, O., S. Kazadzis, M. Blumthaler, L. Ylianttila, B. Johnsen, K. Lakkala, T. Koskela and W. Josefsson (2006), Diurnal discrepancies in spectral solar UV radiation measurements, Appl. Opt., 45, 5346-5357.

Min, W. L. and L. C. Harrison (1998), Synthetic spectra for terrestrial ultraviolet from discrete measurements. J. Geophys. Res., 103, 17033-17039.

Paulsson, L-E. and U. Wester (eds) (2006), The Nordic intercomparison of ultraviolet and total ozone radiometers at Tylösand, Sweden, in 2000 (manuscript to be published in SSI Reports, 2006). ISSN 0282-4434.

Seckmeyer, G. and G. Bernhard (1993), Cosine Error Correction of spectral UV-irradiances, Proc. SPIE Vol. 2049, p. 140-151, Atmospheric Radiation, K. H. Stamnes; Ed..

Slaper, H., H. A. J. M. Reinen, M. Blumthaler, M. Huber and F. Kuik (1995), Comparing ground-level spectrally resolved solar UV measurements using various instruments: A technique resolving effects of wavelength shift and slit width, Geophysical Research Letters, Vol. 22, No. 20, p. 2721-2724.

Webb, A., J. Gröbner, M. Blumthaler (2006), A practical guide to operating broadband instruments measuring erythemally weighted irradiance, COST Action 726, COST Office, ISBN 92-898-0032-1, 2006.

WHO (2002), Global Solar UV Index: A practical Guide. A joint recommendation of the World Health Organization, World Meteorological Organization, United Nations Environmental Programme, and the International Commission on Non-Ionizing Radiation Protection, World Health Organization WHO/ASW/OEH/02.2.

List of abbreviations

CIE	International Commission on Illumination
CMS	Calibration Measurement Software solutions
CMS150	the DM150 spectroradiometer from CMS
CLOD	UVA Cloud Optical Depth
COST	European Co-operation in the Field of Scientific and Technical Research
DM150	Spectroradiometer model DM150 from Bentham Instruments Ltd
DTM300	Spectroradiometer model DTM300 from Bentham Instruments Ltd
FARIN	Factors Controlling UV Radiation In Norway
FWHM	Full Width at Half Maximum
GCCF	Global Cosine Correction Function
GCR	Global Cosine Ratio = 1/GCCF
GUV	Ground based UV Radiometer
MBFR	Multi Band Filter Radiometer
MFRSR	Multi Filter Rotating Shadowband Radiometer
NILU-UV	Norwegian Institute of Air Research - UV radiometer
NRPA	Norwegian Radiation Protection Authority
NRP150	the DM150 spectroradiometer from NRPA
NRP300	the DTM300 spectroradiometer from NRPA
NTNU	Norwegian University of Science and Technology
NTN150	the DM150 spectroradiometer from NTNU
PAR	Photosynthetic Active Radiation
QASUME	Quality Assurance of Spectral Ultraviolet Measurements in Europe
RT	Radiative Transfer
SZA	Solar Zenith Angle
USDA	United States Department of Agriculture
UVA	Ultraviolet-A band, wavelengths 315-400 nm
UVB	Ultraviolet-B band, wavelengths 280-315 nm
UVI	Global UV Index
WHO	World Health Organization (United Nations)
WMO	World Meteorological Organization (United Nations)

Air temperature (°C), relative humidity, total solar irradiance (W/m^2) and daily total ozone amount (DU) recorded for the core period, day 142-162

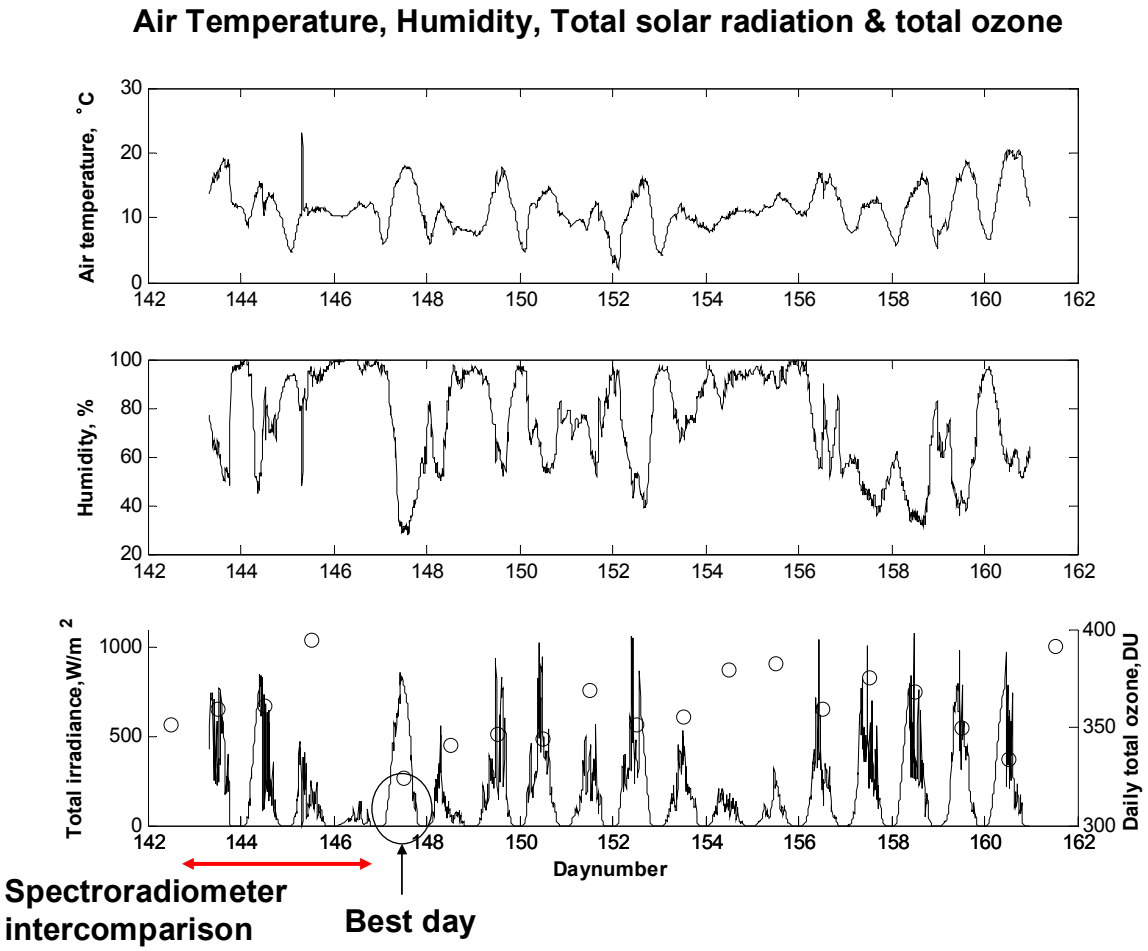

ANNEX A2

Participants representing different groups of radiometers

Spectroradiometers:
Bentham DM150 – Josef Schreder, CMS Ing. Dr Schreder GmbH, Austria, and Mario Blumthaler, Innsbruck Medical University, Austria.

Bentham DM150 – Asadollah Bagheri, Norwegian University of Science and Technology (NTNU), Norway.

Bentham DM150 & Bentham DTM300 – Bjørn Johnsen, Norwegian Radiation Protection Authority (NRPA), Norway.

Brewer MK IV total ozone and UV spectroradiometer operating at the University of Oslo - Arne Dahlback, Dept. of Physics, University of Oslo (UiO), Norway.

Multiband filter radiometers.
GUV- Germar Bernhard, Biospherical Instruments Inc. (BSI), San Diego, USA.
GUV – Tommy Nakken Aalerud, Norwegian Radiation Protection Authority (NRPA), Norway.
GUV – Lars-Erik Paulsson, Swedish Radiation Protection Authority (SSI), Sweden.
GUV – Andrew Smedley, SEAES, University of Manchester (UMIST), UK.

NILU-UV – Britt Ann Høiskar, Norwegian Institute for Air Research (NILU), Norway.
NILU-UV – Chrysanthi Topaloglou, Aristotle University of Thessaloniki (AUTH), Greece.
NILU-UV – Outi Meinander, Finnish Meteorological Institute (FMI), Helsinki, Finland.
NILU-UV – Kaisa Lakkala, Finnish Meteorological Institute (FMI), Sodankylä, Finland.
NILU-UV – Grzegorz Zablocki, Institute of Meteorology and Water Management (IMWM), Poland.
NILU-UV – David Bolsée, Belgian Institute for Space Aeronomy, Belgium.
NILU-UV – Alberto Redondas Marrero, Atmoferico de Izaña, Instituto Nacional de Meteorologia (INM), Spain.

UV-MFRSR (UV multifilter rotating shadowband radiometer) – John Davis, Colorado State University, USDA/UVB Monitoring Programme,USA.

Measurement sites of MBFRs, interlinked with radiometers participating in the MBFR intercomparison:

Europe:
Norway: Oslo, Bergen, Grimstad, Gjøvik, Finse (mountain), Trondheim, Andøya and Ny-Ålesund.
Sweden: Stockholm
Finland: Jokioinen and Helsinki. Travelling standard for Spanish Antarctic UV network.
Belgium.
Spain: Tenerife
Italy: Firenze
Poland: Legionowo
England: Manchester
Greece: Thessaloniki, later implemented in a Greek monitoring network
Germany: Two NILU-UVs, later moved to Russia (locations unknown to the authors).

Antarctica: Belgrano, Marambia, South Pole, Palmer and Queen Maud Land.

South America: Ushuaia in Argentina.

North America: San-Diego, Wallop Island and New-Jersey.

The two MFRSR radiometers of the USDA UV-B monitoring network represent stations at Hawaii, New-Zealand, and USA from Texas to Alaska.

Africa: Uganda, Tanzania and Gambia.

Asia: Khatmandu in Nepal.

Radiometer serial number and literature reference for the processing of UVI by the participants

Radiometer type	Serial number	Literature reference
NILU-UV I	990304	Dahlback, 1996;
NILU-UV I	990310	Dahlback, 1996;
NILU-UV I	990319	Dahlback, 1996;
NILU-UV I	990331	Dahlback, 1996;
NILU-UV I	990339	Dahlback, 1996;
NILU-UV II	04102	Dahlback, 1996;
NILU-UV II	04106	Dahlback, 1996;
GUV-511	9222	Dahlback, 1996;Johnsen et al., 2002
GUV-541	9297	Dahlback, 1996;
GUV-541	9270	Dahlback, 1996;Johnsen et al., 2002
GUV-541	9271	Dahlback, 1996;Johnsen et al., 2002
GUV-541	9272	Dahlback, 1996;Johnsen et al., 2002
GUV-541	9273	Dahlback, 1996;Johnsen et al., 2002
GUV-541	9274	Dahlback, 1996;Johnsen et al., 2002
GUV-541	29222	Dahlback, 1996;Johnsen et al., 2002
GUV-541	29229	Dahlback, 1996;Johnsen et al., 2002
GUV-541	29237	Dahlback, 1996;Johnsen et al., 2002
GUV-541	29243	Dahlback, 1996;Johnsen et al., 2002
GUV-541	9275	Dahlback, 1996;Johnsen et al., 2002
GUV-541	9276	Dahlback, 1996;Johnsen et al., 2002
GUV-541	29233	Dahlback, 1996;
GUV-2511	04123	Dahlback, 1996; Bernhard et al., 2005
GUV-2511	04121	Dahlback, 1996; Bernhard et al., 2005
UV-MFRSR	00286	Min and Harrison, 1998;Davis and Slusser, 2005
UV-MFRSR	00292	Min and Harrison, 1998;Davis and Slusser, 2005

ANNEX A4

Multiband filter radiometers participating in the campaign and the characterization work performed in the laboratory. X denotes that the work has been done

Instrument type	Instrument	S/num	$C(\theta, \varphi)$	$S(\lambda)$	QTH lamps
MBFR	NILU-UV	990331	x	x	-
MBFR	NILU-UV	04102	-	x	-
MBFR	NILU-UV	990304	-	x	-
MBFR	NILU-UV	990310	-	x	-
MBFR	NILU-UV	990339	x	x	-
MBFR	NILU-UV	04106	x	x	-
MBFR	NILU-UV	04108	-	x	-
MBFR	NILU-UV	04109	-	x	-
MBFR	NILU-UV	04110	-	x	-
MBFR	NILU-UV	04111	-	x	-
MBFR	NILU-UV	04114	-	x	-
MBFR	NILU-UV	04115	-	x	-
MBFR	NILU-UV	04116	-	x	-
MBFR	NILU-UV	04117	-	x	-
MBFR	NILU-UV	04118	x	x	-
MBFR	NILU-UV	04120	-	x	-
MBFR	NILU-UV	990319	x	x	-
MBFR	NILU-UV	990306	-	x	-
MBFR	NILU-UV	990313	-	x	-
MBFR	NILU-UV	990325	-	x	-
MBFR	NILU-UV	990327	-	x	-
MBFR	NILU-UV	990329	-	x	-
MBFR	NILU-UV	990338	-	x	-
MBFR	NILU-UV	04112	-	x	-
MBFR	NILU-UV	04113	x	x	-
MBFR	GUV-541	9297	x	x	x
MBFR	GUV-2511	04123	x	x	x
MBFR	GUV-2511	04121	x	x	x
MBFR	GUV-541	9270	x	x	x
MBFR	GUV-541	9271	x	x	x
MBFR	GUV-541	9272	x	x	x
MBFR	GUV-541	9273	x	x	x

Instrument type	Instrument	S/num	$C(\theta, \varphi)$	$S(\lambda)$	QTH lamps
MBFR	GUV-541	9274	x	x	x
MBFR	GUV-541	29222	x	x	x
MBFR	GUV-541	29229	x	x	x
MBFR	GUV-541	29237	x	x	x
MBFR	GUV-541	29243	x	x	x
MBFR	GUV-541	9275	x	x	x
MBFR	GUV-541	9276	x	x	x
MBFR	GUV-511	9222	x	x	x
MBFR	GUV-541	29233	x	x	x
MBFR	UV-MFRSR	00286	x	x	-
MBFR	UV-MFRSR	00292	x	x	-

ANNEX A5

Empirical corrections of the relative spectral responsivity functions. A case study for GUV serial number 9270

The peak-normalized spectral response function of each detector channel was assembled from series of measurements, with the excitation monochromators set to different bandwidths (ref. section 2.6.1). This first approximation of the true responsivity function $r_i^{(0)}$ was next tested against global sky measurements with the MBFR and spectroradiometer-based simulations of the detector output (Eq. 6). Modifications were made to $r_i^{(0)}$ until the response factors K_i (Eq. 6) were acceptable constant (±2%) for all SZAs. Prior to the calculations, the influences from cosine errors resulting from non-ideal angular responsivity functions were corrected, applying GCCF in section 2.7 (see eg. GCCF vs. SZA in Figure 17). The response factors $K_i^{(0)}$ resulting from this first approximation are shown in Figure A5.1 for the five detector channels of GUV 9270, as a function of SZA. As may be seen, cosine corrections (open symbols) resulted in factors that were less SZA-dependent and less dependent on the solar azimuth (red and blue symbols) than without the use of cosine corrections (solid symbols). However, it may be seen that the Ki's for the first channel have a significant slope, indicating that $r_i^{(0)}$ poorly matches the true responsivity function of the radiometer.

The SZA-dependency in Ki's results from errors in $r_i^{(0)}$ related to the laboratory set-up, and possibly also effects from differences in the spectral and directional distribution of the laboratory source and global sky. Candidate error sources are 1) errors in the wavelength scale of the monochromatic excitation source or wavelength shifts induced by the directional distribution of the source, 2) convolution effects resulting from finite bandwidths of the excitation source, 3) existence of secondary responsivity peaks and finite responses at high wavelengths that could not be resolved in the laboratory, due to limited dynamic response of the detector signals, and 4) non-linear response to the intensity of the excitation source.

Influence of small wavelength errors in ri: The introduction of a shift in the wavelength scale of r_i may help to compensate the SZA-dependency in Ki for those channels overlapping the solar cut-off region ($\lambda < 325$ nm) In Figure A5.2 we added -0.2 nm to the wavelength scale of detector channel 1 (305 nm), whereas the scales of the other channels were unshifted. As may be seen, most of the SZA dependency of channel 1 was compensated (within ±2% up to SZA 70°). However, a shift by -0.2 nm is unlikely large in our case, as measurements of the slit functions at all wavelength settings from 270nm to 420 nm showed maximum errors less than ±0.1 nm. Hence, other error sources may have larger significance than errors in the wavelength scale.

Effects from finite bandwidths of the excitation source: Bernhard et al. [2005] have shown that the broadening in r_i resulting from finite bandwidths of the excitation monochromator may be partly corrected, using an approximated deconvolution algorithm:

$$R_{deconv}(\lambda) = U^2_{measured}(\lambda) / U_{conv}(\lambda)$$

where R_{deconv} is the deconvoluted responsivity function, $U_{measured}$ is the output signal measured for the actual slit function, and U_{conv} is the output signal convoluted with the slit function of the excitation monochromators. The Ki's resulting from deconvolution of ri's are shown in Figure A5.3. The enhanced steepness in flanges of r_i resulted in significantly smaller SZA-dependency of K_i for the channel 1 (305 nm), as did also the addition of a negative wavelength shift in the previous case (Figure A5.2). The Ki's for the other channels were almost unaffected. In order to further reduce the SZA-dependency, the steepness of deconvoluted ri's were enhanced by multiplying the wavelength scale around the steepest region of ri with a factor γ smaller or larger than 1.00 and interpolating ri back to the original sampling wavelengths. Choosing γ equal to 0.90 for the first 3 channels' response functions resulted in Ki's that were almost within ±2% for all SZA's, as may be seen in Figure A5.4.

Influences from finite responses at large wavelengths. Secondary peaks and finite responses at large wavelengths are manifested in Ki for moderate and high SZAs (60° or more). If Ki's increase with increasing SZA, the initially determined response factors are too small at large wavelengths compared with the true radiometer response. Inclusion of a response-tail that is too high in the UVA for channel 1 result in Ki's that fall off at high SZA, as shown in Figure A5.5.

The final Ki's resulting from optimal modifications of ri is shown in Figure A5.6. Residual deviations may be due to uncertainties in the cosine corrections and effects from other response functions. The final spectral response functions are shown in Figure A5.7. The initial response functions r_i^0 were first deconvoluted and further made steeper with the γ set to 0.9. A UVA tail equal to 10^{-6} was added to the channel 1, and the magnitude of the secondary peaks of channel 2 and 3 reduced by a factor 1.05.

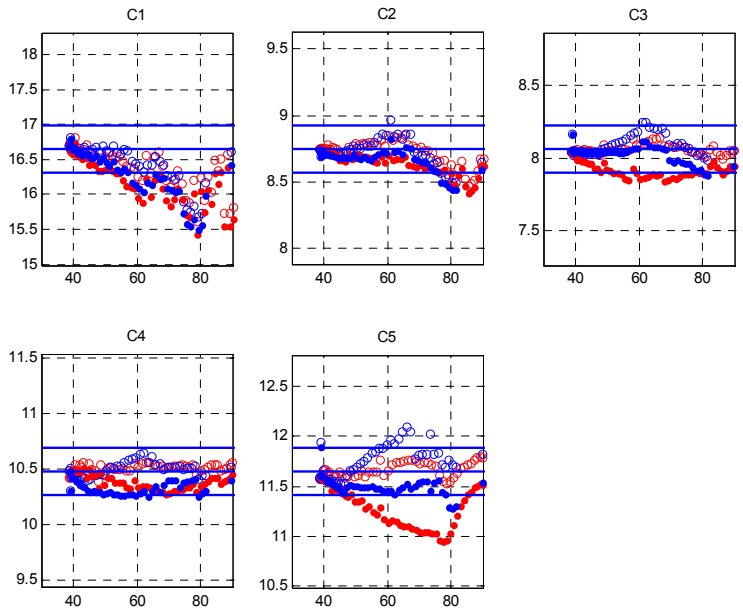

Figure. A5.1. Absolute responsivity factors K_i (Y-axis) as function of SZA (X-axis) for GUV 9273 for day of year 147 2005, applying the original peak-normalized responsivity functions from laboratory characterizations ($r_i^{(0)}$). Red and blue symbols correspond to rising and setting sun. Open and solid symbols correspond to Ki's obtained respectively with and without cosine corrections of the detector outputs. Horizontal lines represent to ±2% intervals in the mean K_i. The reference spectroradiometer is DTM300.

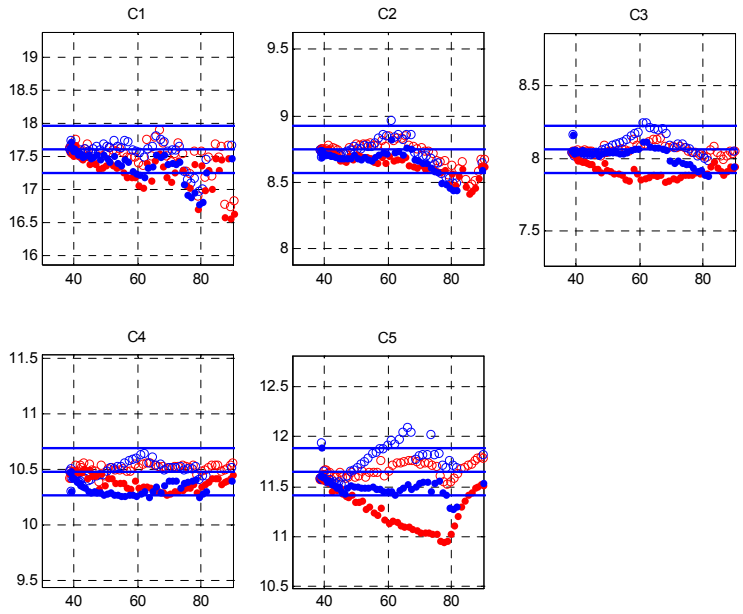

Figure A5.2. **Same as Figure A5.1, but wavelength scale of the spectral responsivity function of detector channel 1 shifted by -0.2 nm.**

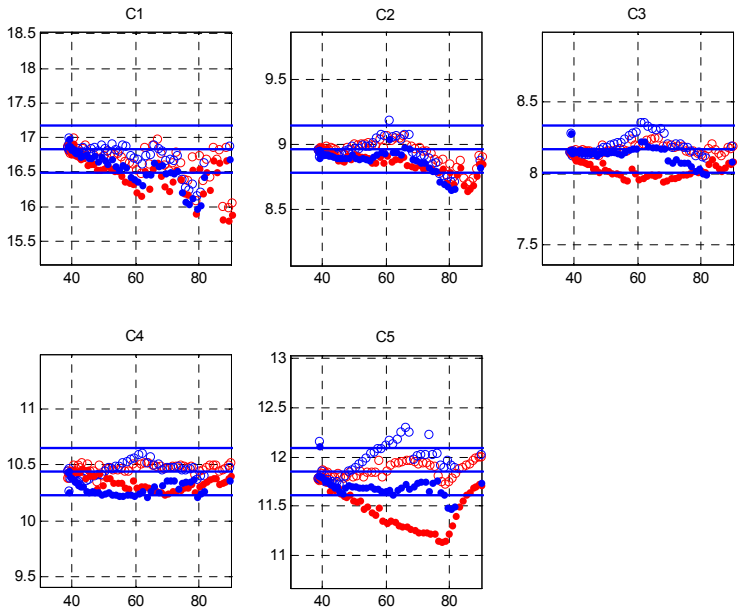

Figure A5.3. **Same as Figure A5.1, but with the spectral responsivity function deconvoluted.**

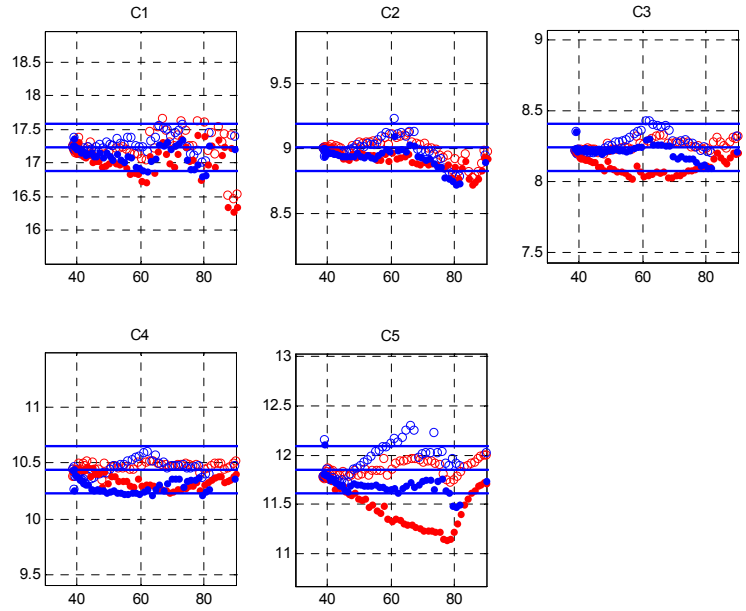

Figure A5.4. **Same as Figure A5.3, but with steepness of deconvolved responsivity functions enhanced with a constant factor for channels 1 to 3.**

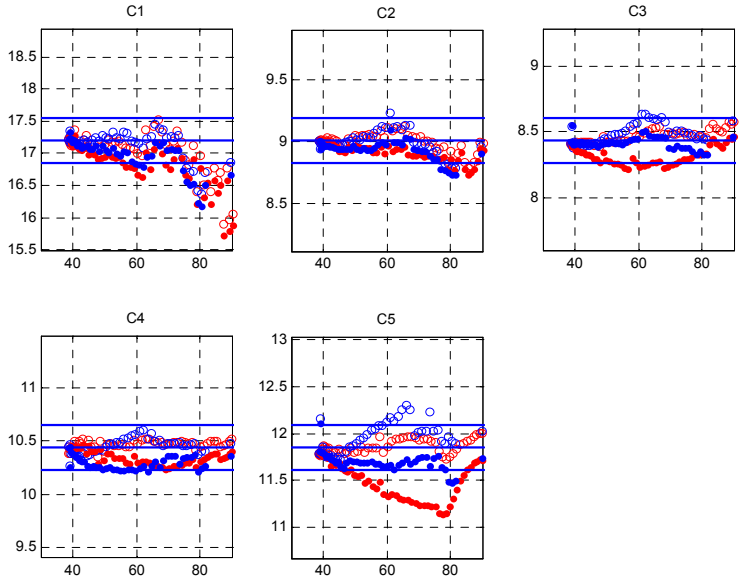

Figure A5.5. **Same as Figure A5.4, but for a response tail in the UVA of channel 1 set too high (equal to 10^{-5}).**

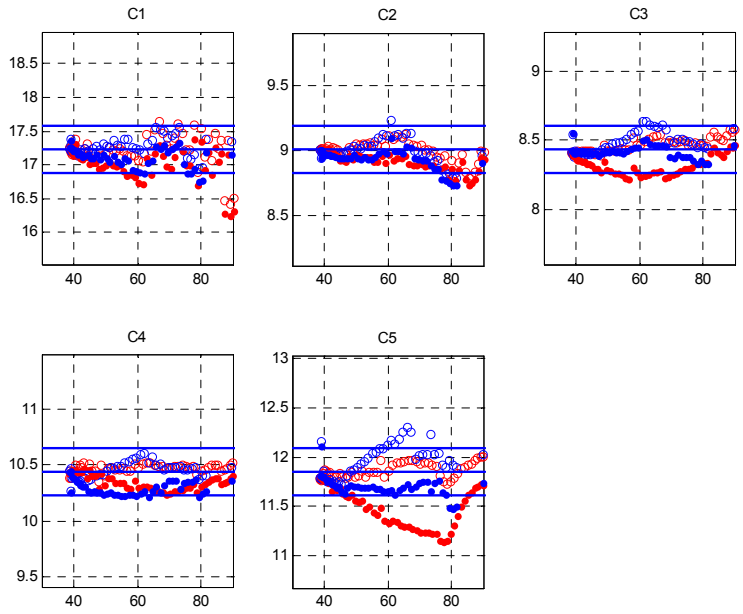

Figure A5.6. **Ki's resulting from deconvolution, sharpening of flanges and inclusion and modification of the magnitude of secondary response peaks in the initial spectral response function ri.**

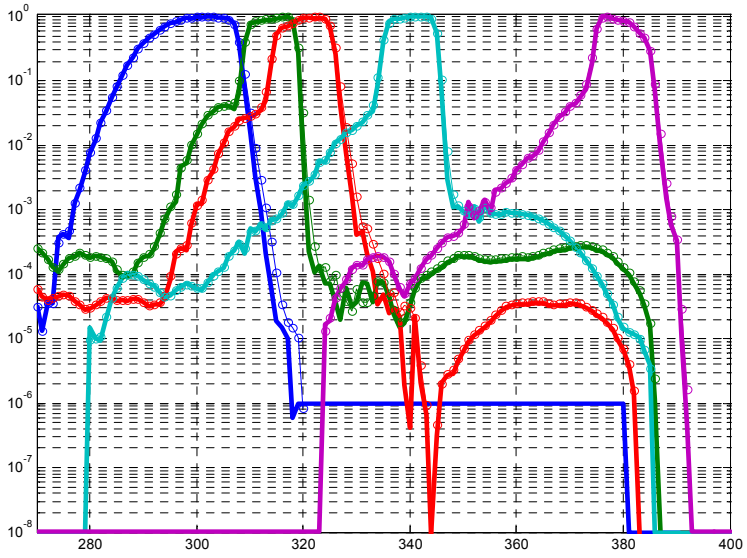

Figure A5.7. **The initial spectral response functions from laboratory characterizations (circles) and the results after modifications (thick lines).**

UVI results provided by the participants and harmonized UVI results relative to the campaign spectral reference, for the period day 140 to 160 2005

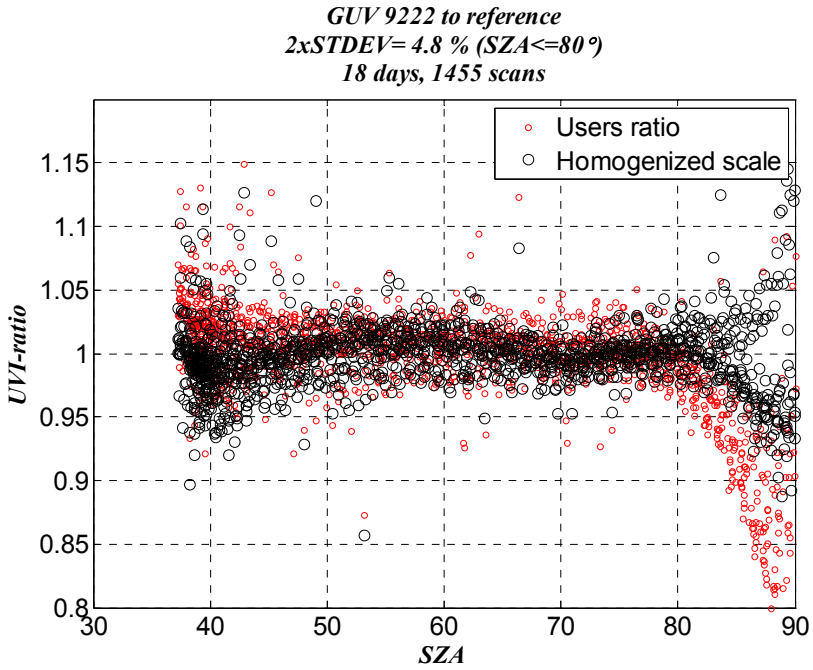

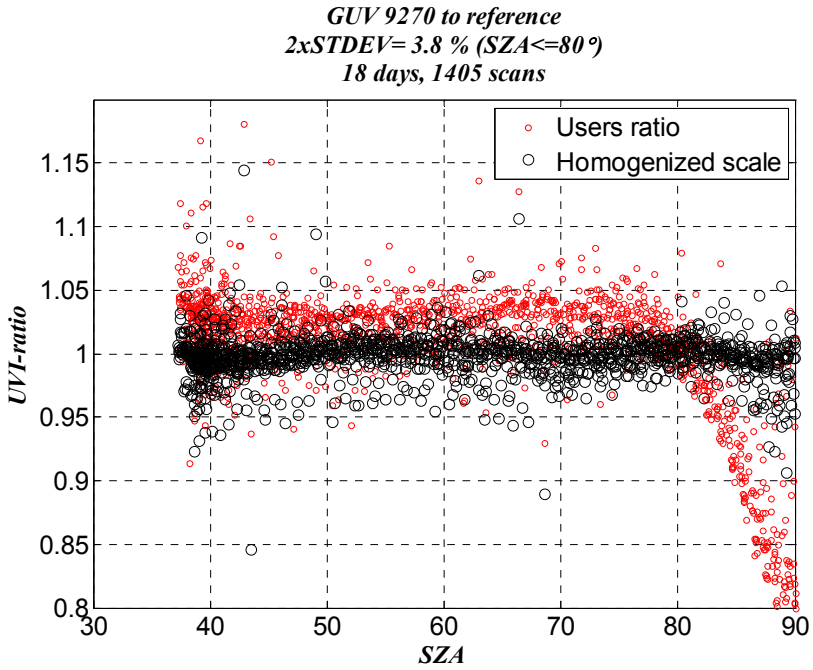

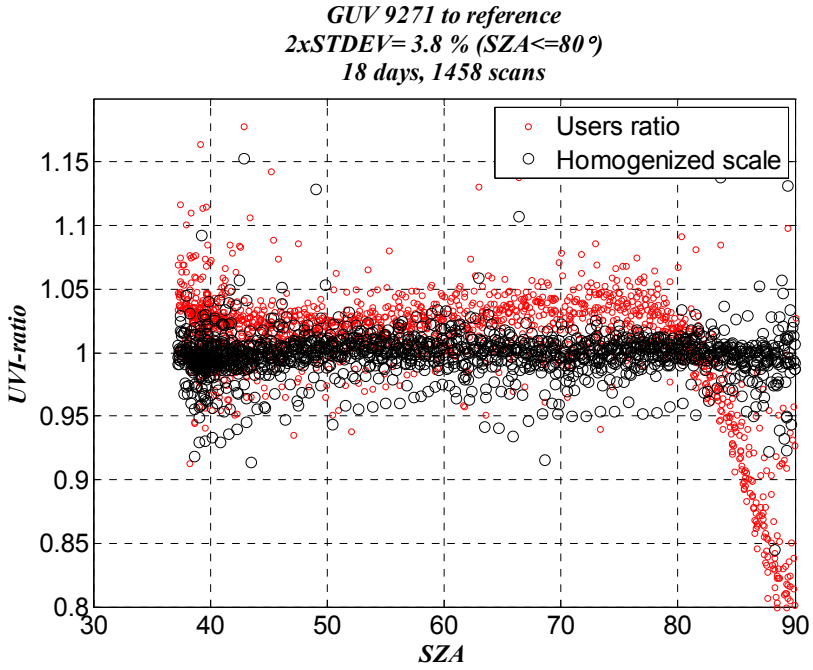
GUV 9271 to reference
2xSTDEV= 3.8 % (SZA<=80°)
18 days, 1458 scans
Users ratio
Homogenized scale
UVI-ratio
SZA
1.15
1.1
1.05
1
0.95
0.9
0.85
0.8
30
40
50
60
70
80
90

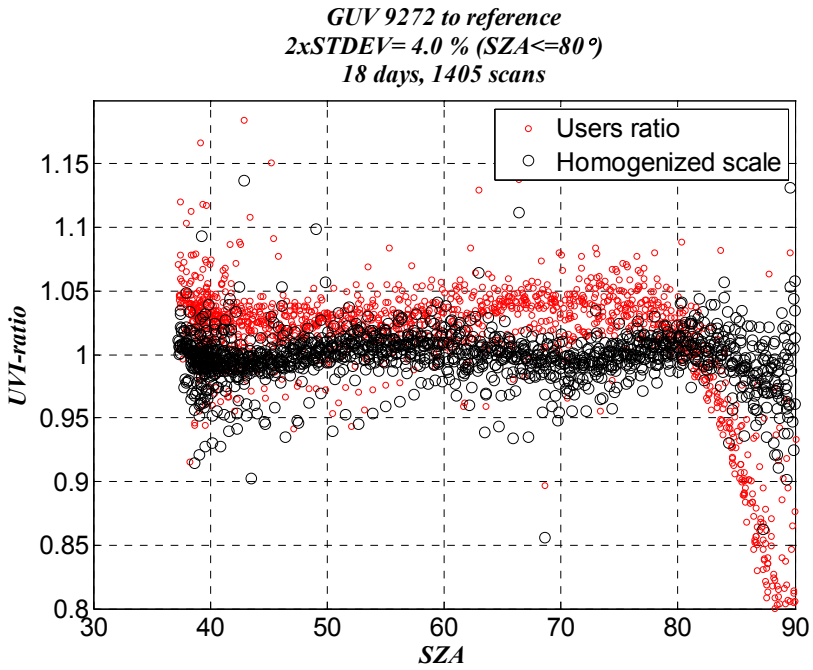
GUV 9272 to reference
2xSTDEV= 4.0 % (SZA<=80°)
18 days, 1405 scans
Users ratio
Homogenized scale
UVI-ratio
SZA
1.15
1.1
1.05
1
0.95
0.9
0.85
0.8
30
40
50
60
70
80
90

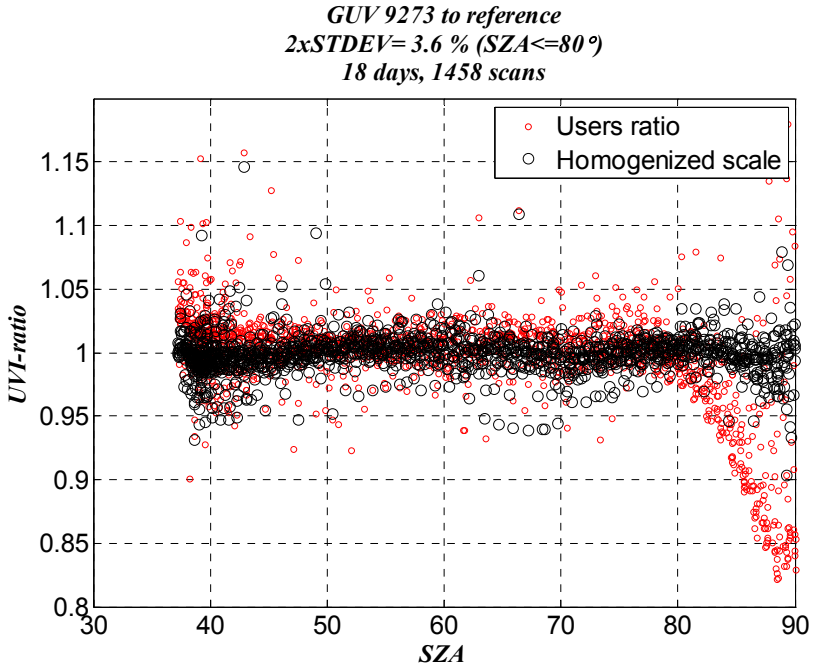
GUV 9273 to reference
2xSTDEV= 3.6 % (SZA<=80°)
18 days, 1458 scans
Users ratio
Homogenized scale
UVI-ratio
SZA
1.15
1.1
1.05
1
0.95
0.9
0.85
0.8
30
40
50
60
70
80
90

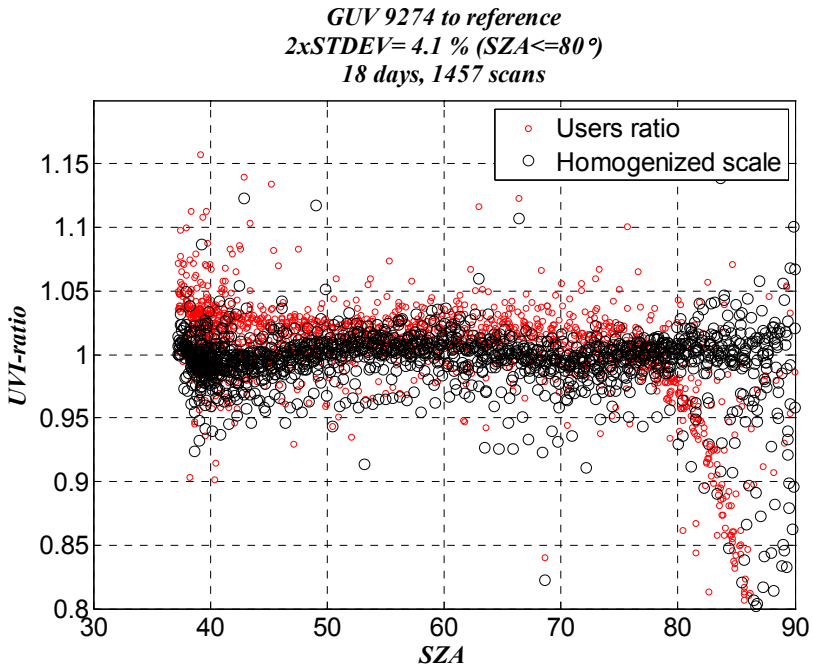
GUV 9274 to reference
2xSTDEV= 4.1 % (SZA<=80°)
18 days, 1457 scans
Users ratio
Homogenized scale
UVI-ratio
SZA
1.15
1.1
1.05
1
0.95
0.9
0.85
0.8
30
40
50
60
70
80
90

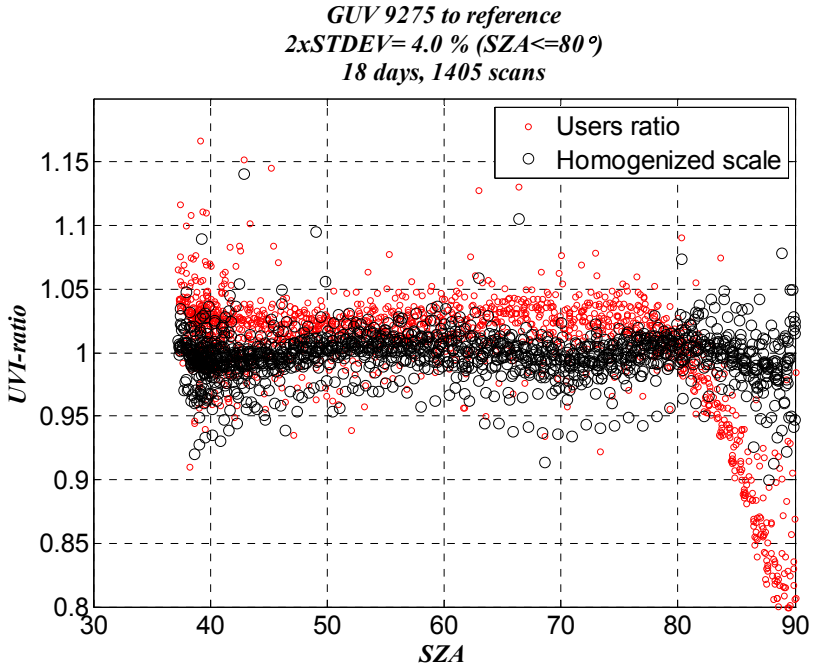
GUV 9275 to reference
2xSTDEV= 4.0 % (SZA<=80°)
18 days, 1405 scans
Users ratio
Homogenized scale
UVI-ratio
SZA
1.15
1.1
1.05
1
0.95
0.9
0.85
0.8
30
40
50
60
70
80
90

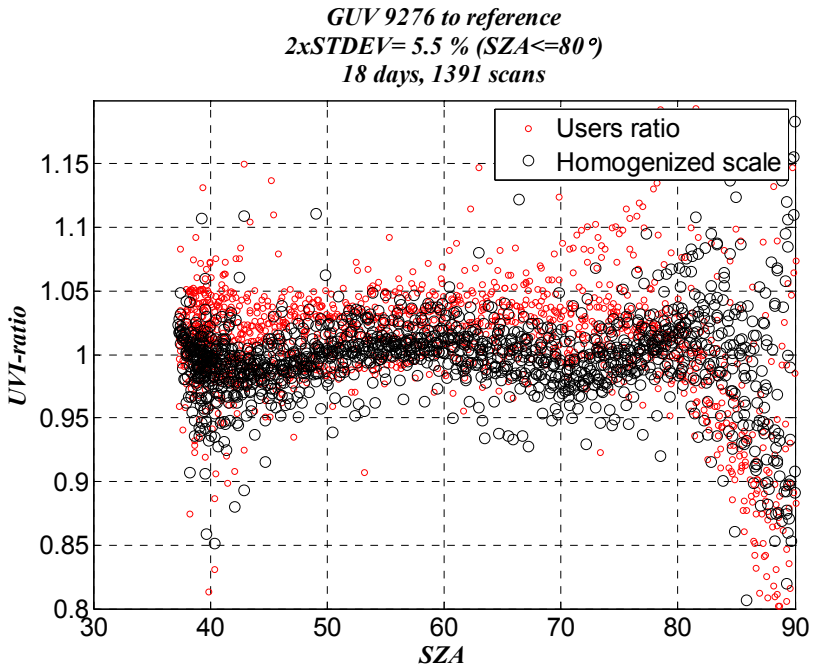
GUV 9276 to reference
2xSTDEV= 5.5 % (SZA<=80°)
18 days, 1391 scans
Users ratio
Homogenized scale
UVI-ratio
SZA
1.15
1.1
1.05
1
0.95
0.9
0.85
0.8
30
40
50
60
70
80
90

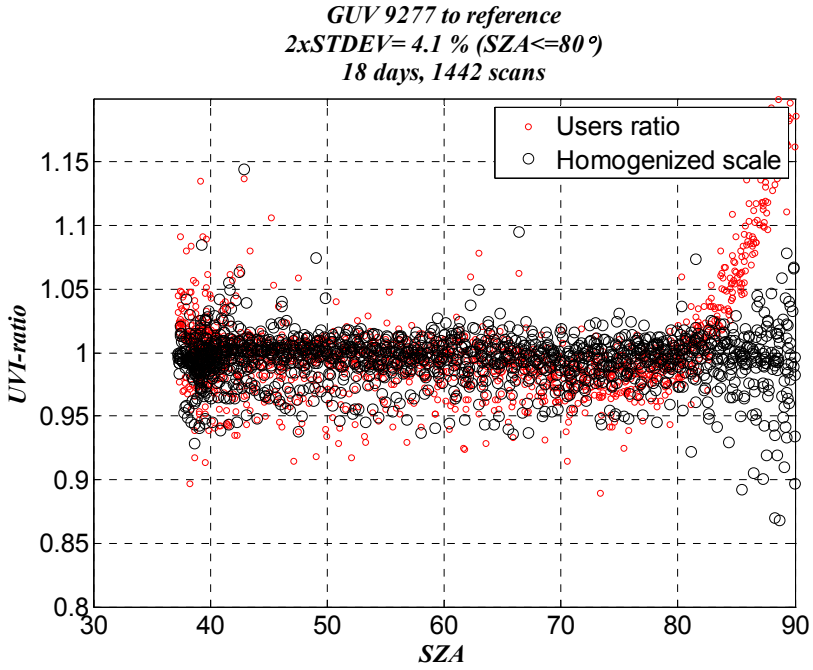
GUV 9277 to reference
2xSTDEV= 4.1 % (SZA<=80°)
18 days, 1442 scans
Users ratio
Homogenized scale
UVI-ratio
SZA
1.15
1.1
1.05
1
0.95
0.9
0.85
0.8
30
40
50
60
70
80
90

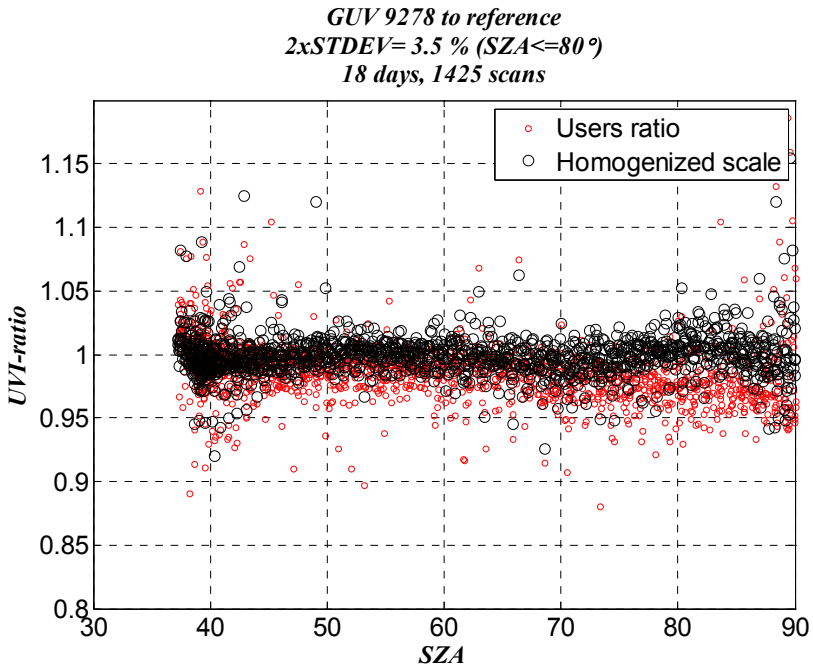
GUV 9278 to reference
2xSTDEV= 3.5 % (SZA<=80°)
18 days, 1425 scans
Users ratio
Homogenized scale
UVI-ratio
SZA
1.15
1.1
1.05
1
0.95
0.9
0.85
0.8
30
40
50
60
70
80
90

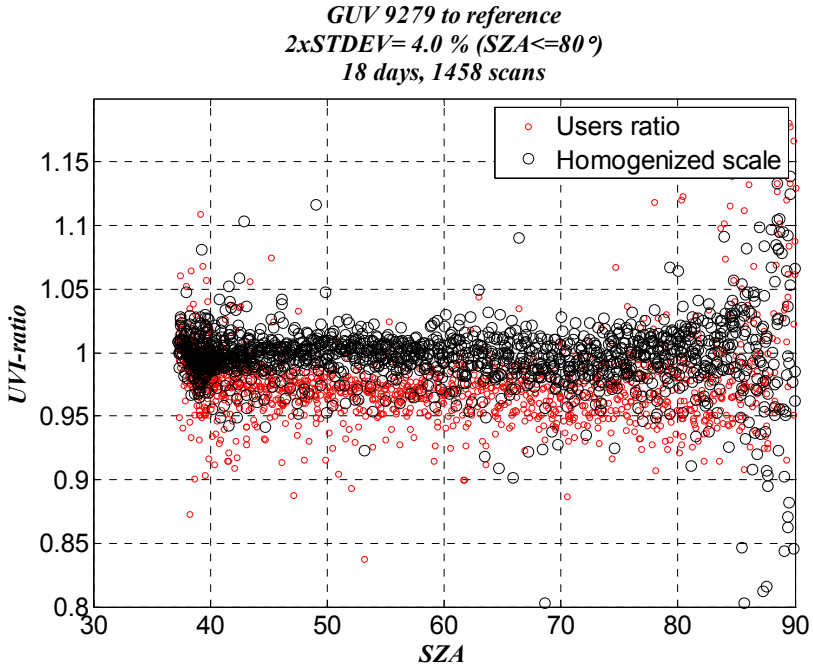
GUV 9279 to reference
2xSTDEV= 4.0 % (SZA<=80°)
18 days, 1458 scans
Users ratio
Homogenized scale
UVI-ratio
SZA
1.15
1.1
1.05
1
0.95
0.9
0.85
0.8
30
40
50
60
70
80
90

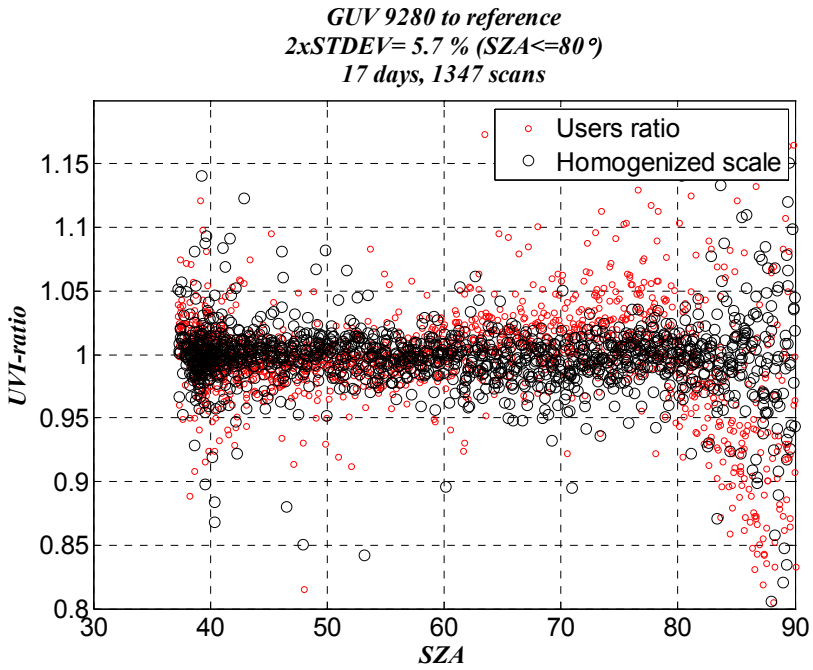
GUV 9280 to reference
2xSTDEV= 5.7 % (SZA<=80°)
17 days, 1347 scans
Users ratio
Homogenized scale
UVI-ratio
SZA
1.15
1.1
1.05
1
0.95
0.9
0.85
0.8
30
40
50
60
70
80
90

GUV 9297 to reference
2xSTDEV= 3.7 % (SZA<=80°)
12 days, 902 scans

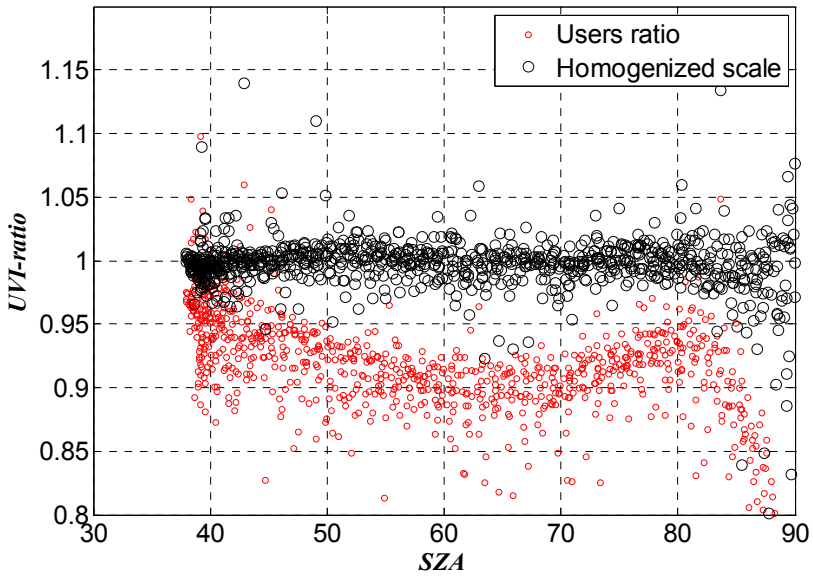

GUV 4123 to reference. User's UVI based on channels 2 to 5 and a choice of coefficients. 2 σ = 4.4% (SZA ≤ 80°), 12 days, 995 scans

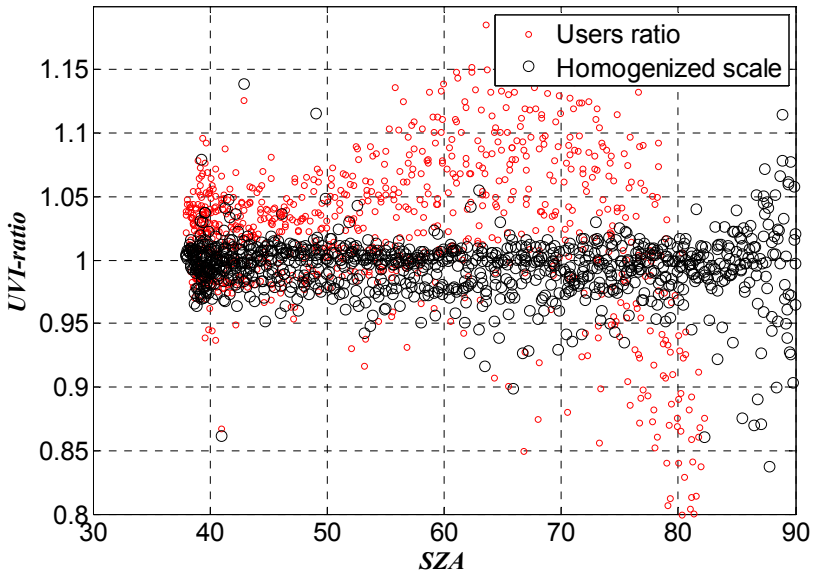

GUV 4123 to reference. User's UVI based on channels 1, 3 to 5 and different choice of coefficients. 2 σ = 4.4% (SZA ≤ 80°).

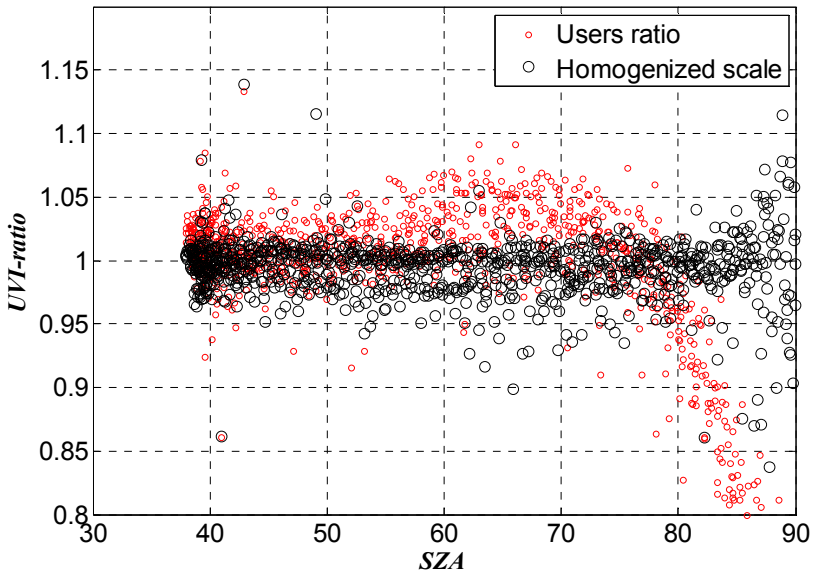

GUV 4121 to reference
2xSTDEV= 4.6 % (SZA<=80°)
14 days, 1043 scans

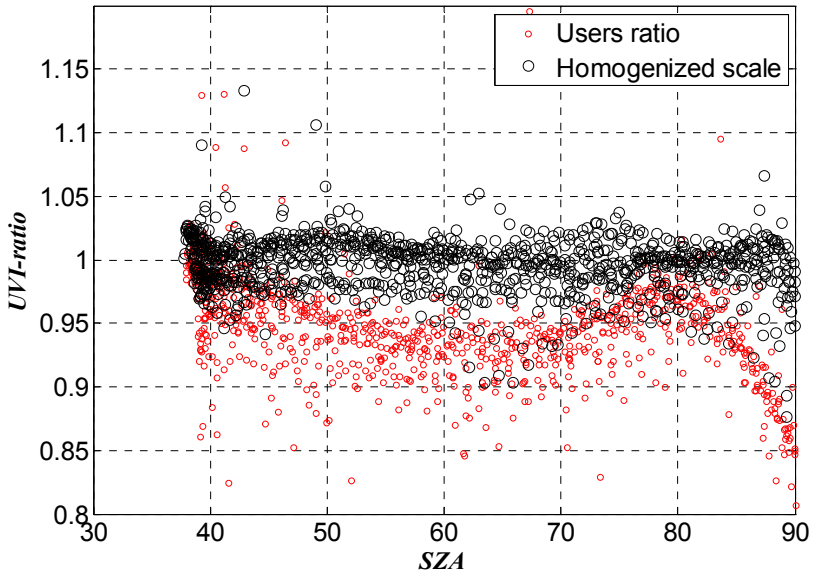

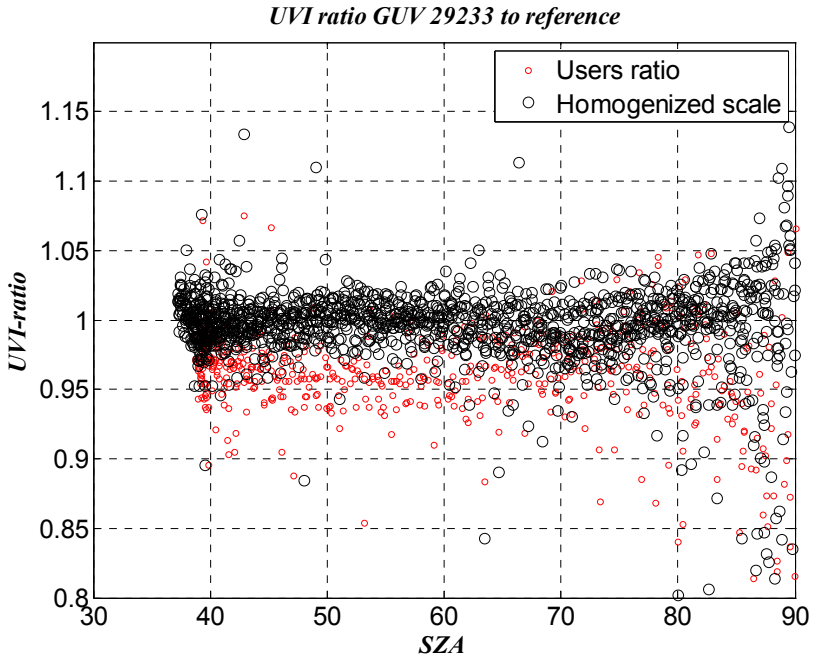
UVI ratio GUV 29233 to reference
Users ratio
Homogenized scale
UVI-ratio
SZA
1.15
1.1
1.05
1
0.95
0.9
0.85
0.8
30
40
50
60
70
80
90

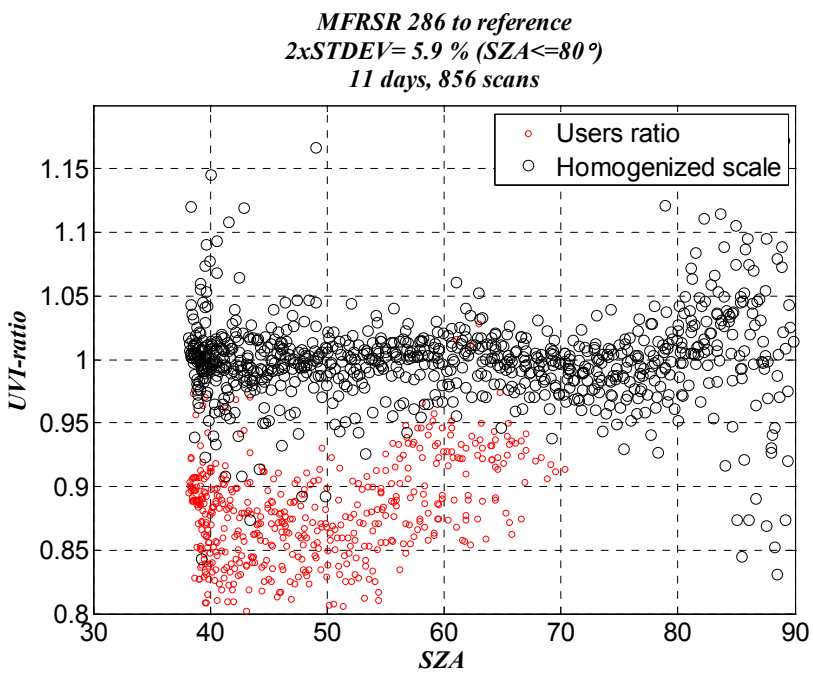
MFRSR 286 to reference
2xSTDEV= 5.9 % (SZA<=80°)
11 days, 856 scans
Users ratio
Homogenized scale
UVI-ratio
SZA
1.15
1.1
1.05
1
0.95
0.9
0.85
0.8
30
40
50
60
70
80
90

MFRSR 292 to reference
2xSTDEV= 8.6 % (SZA<=80°)
10 days, 690 scans

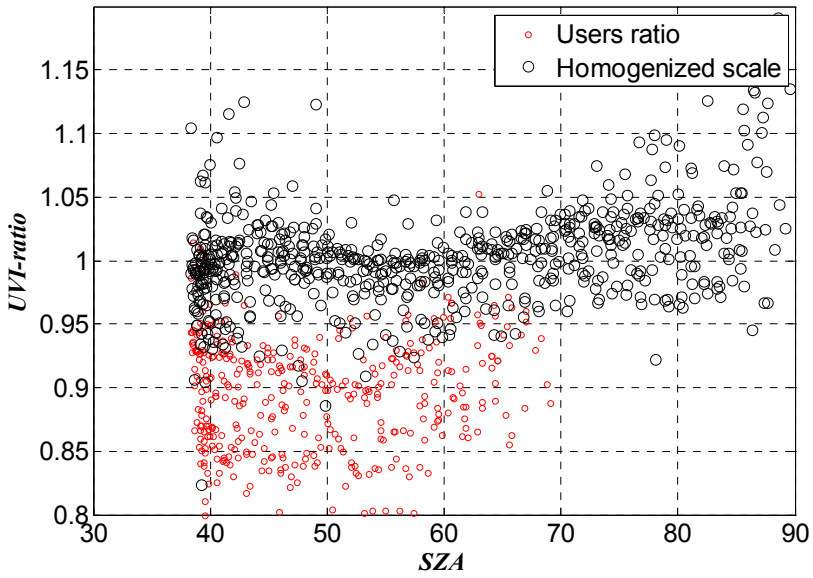

NILUV 990304 to reference
2xSTDEV= 4.0 % (SZA<=80°)
12 days, 972 scans

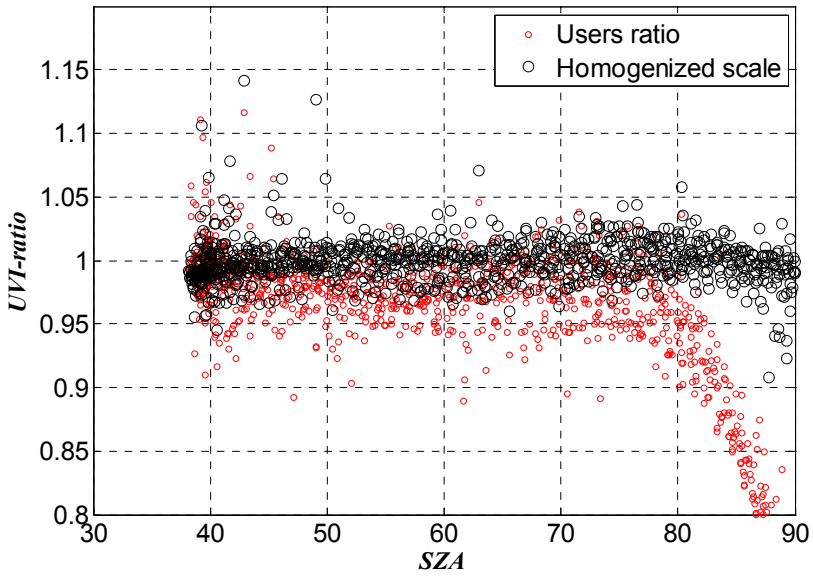

NILUV 990310 to reference
2xSTDEV= 4.4 % (SZA<=80°)
12 days, 971 scans

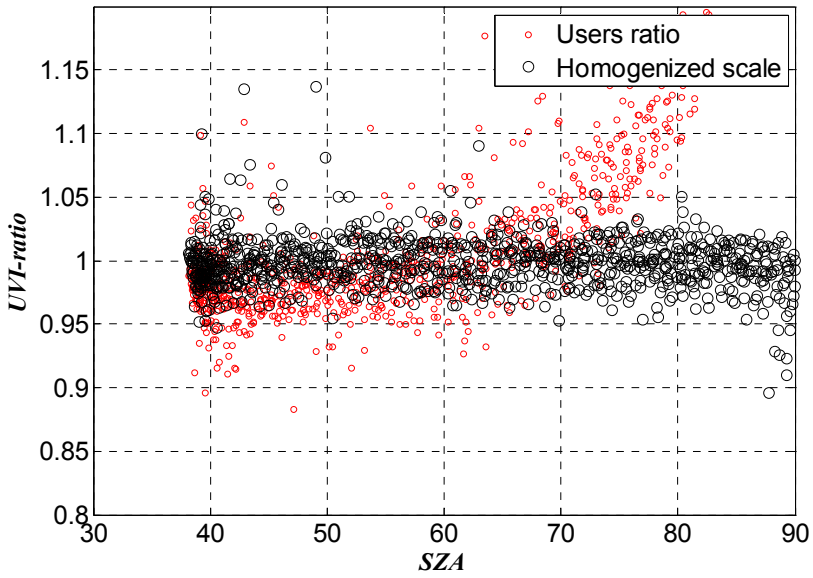

NILUV 990319 to reference
2xSTDEV= 3.8 % (SZA<=80°)
12 days, 972 scans

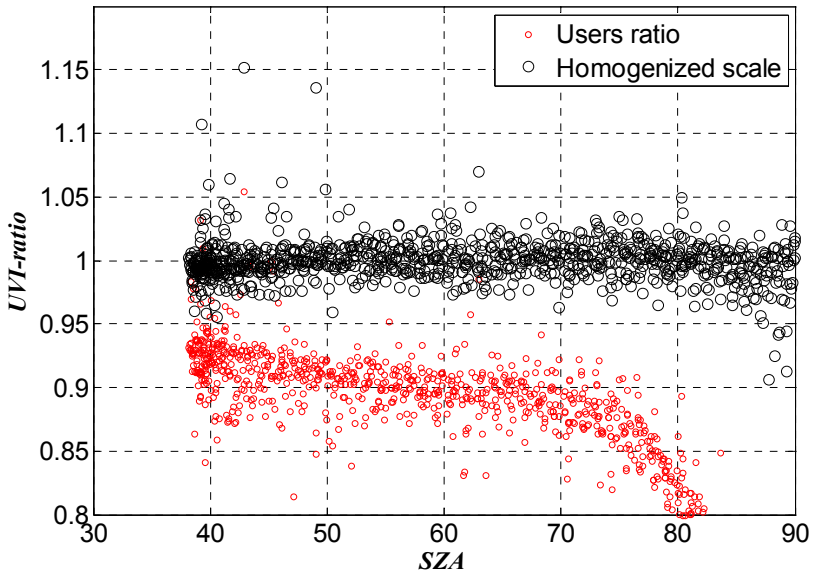

NILUV 990331 to reference
2xSTDEV= 3.7 % (SZA<=80°)
12 days, 974 scans

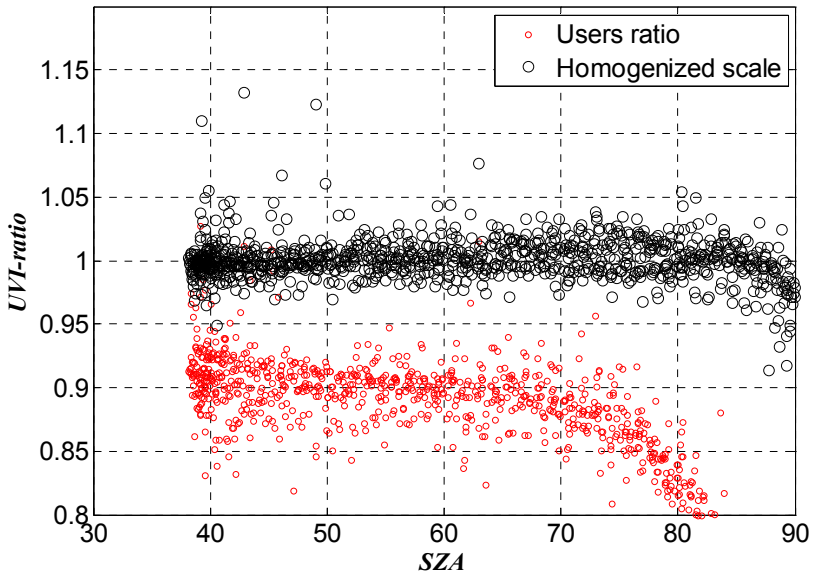

NILUV 990339 to reference
2xSTDEV= 5.2 % (SZA<=80°)
12 days, 974 scans

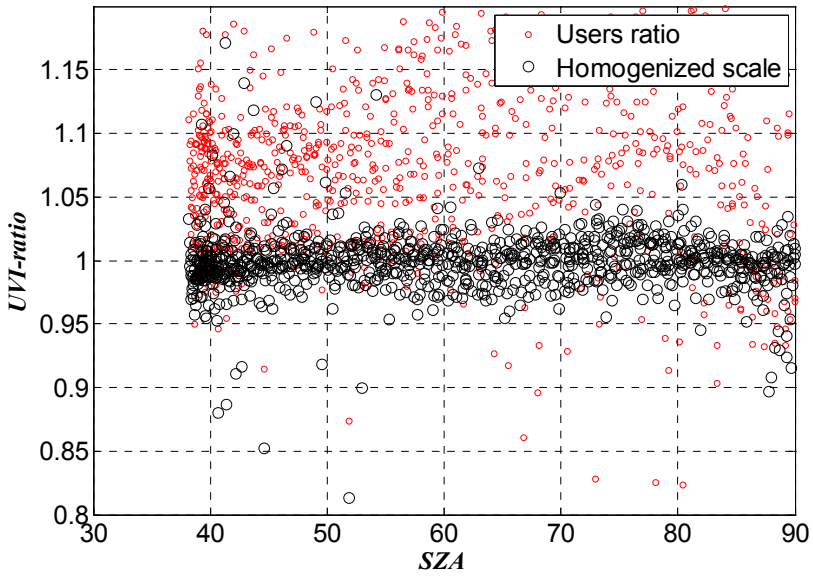

NILUV 4102 to reference
2xSTDEV= 4.8 % (SZA<=80°)
12 days, 975 scans

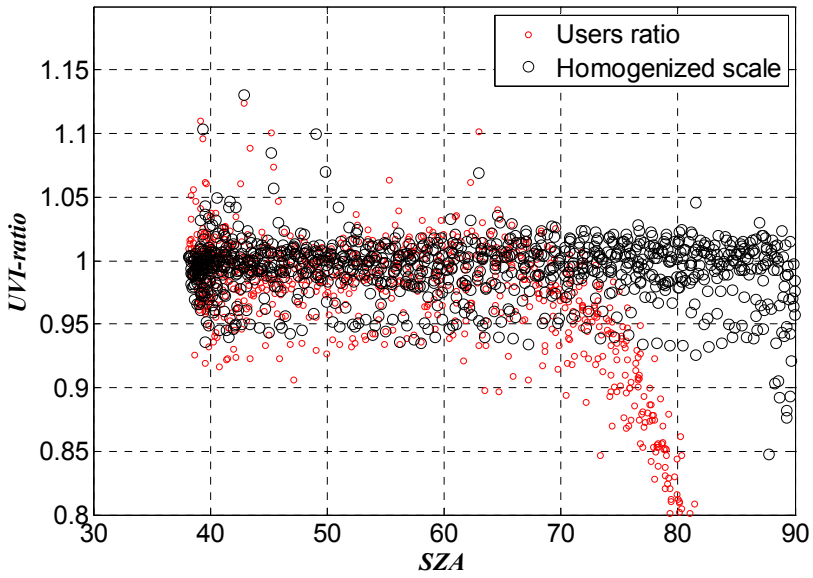

NILUV 4106 to reference
2xSTDEV= 5.7 % (SZA<=80°)
12 days, 972 scans

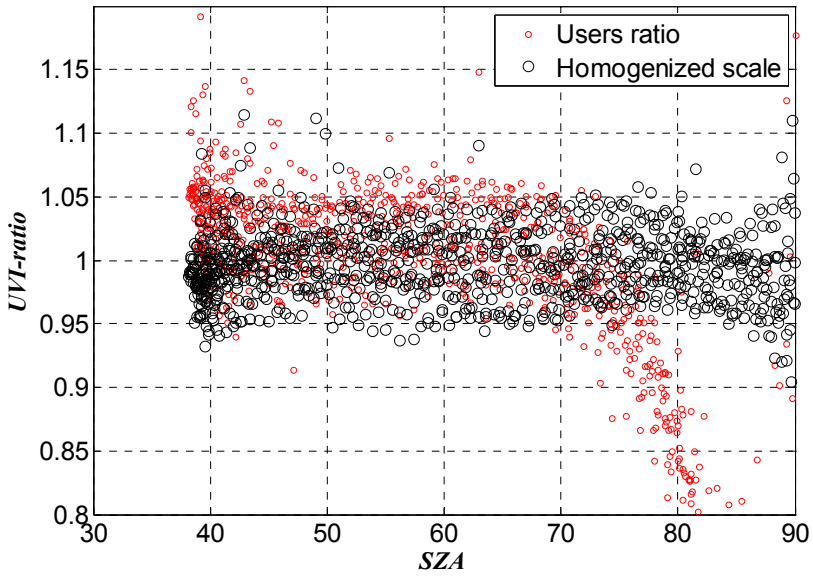

GLOBAL ATMOSPHERE WATCH REPORT SERIES

1. Final Report of the Expert Meeting on the Operation of Integrated Monitoring Programmes, Geneva, 2 -5 September 1980.

2. Report of the Third Session of the GESAMP Working Group on the Interchange of Pollutants Between the Atmosphere and the Oceans (INTERPOLL-III), Miami, USA, 27-31 October 1980.

3. Report of the Expert Meeting on the Assessment of the Meteorological Aspects of the First Phase of EMEP, Shinfield Park, U.K., 30 March - 2 April 1981.

4. Summary Report on the Status of the WMO Background Air Pollution Monitoring Network as at April 1981.

5. Report of the WMO/UNEP/ICSU Meeting on Instruments, Standardization and Measurements Techniques for Atmospheric CO_2, Geneva, 8-11; September 1981.

6. Report of the Meeting of Experts on BAPMoN Station Operation, Geneva, 23–26 November 1981.

7. Fourth Analysis on Reference Precipitation Samples by the Participating World Meteorological Organization Laboratories by Robert L. Lampe and John C. Puzak, December 1981.

8. Review of the Chemical Composition of Precipitation as Measured by the WMO BAPMoN by Prof. Dr Hans-Walter Georgii, February 1982.

9. An Assessment of BAPMoN Data Currently Available on the Concentration of CO_2 in the Atmosphere by M.R. Manning, February 1982.

10. Report of the Meeting of Experts on Meteorological Aspects of Long-range Transport of Pollutants, Toronto, Canada, 30 November - 4 December 1981.

11. Summary Report on the Status of the WMO Background Air Pollution Monitoring Network as at May 1982.

12. Report on the Mount Kenya Baseline Station Feasibility Study edited by Dr Russell C. Schnell.

13. Report of the Executive Committee Panel of Experts on Environmental Pollution, Fourth Session, Geneva, 27 September - 1 October 1982.

14. Effects of Sulphur Compounds and Other Pollutants on Visibility by Dr R.F. Pueschel, April 1983.

15. Provisional Daily Atmospheric Carbon Dioxide Concentrations as Measured at BAPMoN Sites for the Year 1981, May 1983.

16. Report of the Expert Meeting on Quality Assurance in BAPMoN, Research Triangle Park, North Carolina, USA, 17-21 January 1983.

17. General Consideration and Examples of Data Evaluation and Quality Assurance Procedures Applicable to BAPMoN Precipitation Chemistry Observations by Dr Charles Hakkarinen, July 1983.

18. Summary Report on the Status of the WMO Background Air Pollution Monitoring Network as at May 1983.

19. Forecasting of Air Pollution with Emphasis on Research in the USSR by M.E. Berlyand, August 1983.

20. Extended Abstracts of Papers to be Presented at the WMO Technical Conference on Observation and Measurement of Atmospheric Contaminants (TECOMAC), Vienna, 17-21 October 1983.

21. Fifth Analysis on Reference Precipitation Samples by the Participating World Meteorological Organization Laboratories by Robert L. Lampe and William J. Mitchell, November 1983.

22. Report of the Fifth Session of the WMO Executive Council Panel of Experts on Environmental Pollution, Garmisch-Partenkirchen, Federal Republic of Germany, 30 April - 4 May 1984 (WMO TD No. 10).

23. Provisional Daily Atmospheric Carbon Dioxide Concentrations as Measured at BAPMoN Sites for the Year 1982. November 1984 (WMO TD No. 12).

24. Final Report of the Expert Meeting on the Assessment of the Meteorological Aspects of the Second Phase of EMEP, Friedrichshafen, Federal Republic of Germany, 7-10 December 1983. October 1984 (WMO TD No. 11).

25. Summary Report on the Status of the WMO Background Air Pollution Monitoring Network as at May 1984. November 1984 (WMO TD No. 13).

26. Sulphur and Nitrogen in Precipitation: An Attempt to Use BAPMoN and Other Data to Show Regional and Global Distribution by Dr C.C. Wallén. April 1986 (WMO TD No. 103).

27. Report on a Study of the Transport of Sahelian Particulate Matter Using Sunphotometer Observations by Dr Guillaume A. d'Almeida. July 1985 (WMO TD No. 45).

28. Report of the Meeting of Experts on the Eastern Atlantic and Mediterranean Transport Experiment ("EAMTEX"), Madrid and Salamanca, Spain, 6-8 November 1984.

29. Recommendations on Sunphotometer Measurements in BAPMoN Based on the Experience of a Dust Transport Study in Africa by Dr Guillaume A. d'Almeida. September 1985 (WMO TD No. 67).

30. Report of the Ad-hoc Consultation on Quality Assurance Procedures for Inclusion in the BAPMoN Manual, Geneva, 29-31 May 1985.

31. Implications of Visibility Reduction by Man-Made Aerosols (Annex to No. 14) by R.M. Hoff and L.A. Barrie. October 1985 (WMO TD No. 59).

32. Manual for BAPMoN Station Operators by E. Meszaros and D.M. Whelpdale. October 1985 (WMO TD No. 66).

33. Man and the Composition of the Atmosphere: BAPMoN - An international programme of national needs, responsibility and benefits by R.F. Pueschel, 1986.

34. Practical Guide for Estimating Atmospheric Pollution Potential by Dr L.E. Niemeyer. August 1986 (WMO TD No. 134).

35. Provisional Daily Atmospheric CO_2 Concentrations as Measured at BAPMoN Sites for the Year 1983. December 1985 (WMO TD No. 77).

36. Global Atmospheric Background Monitoring for Selected Environmental Parameters. BAPMoN Data for 1984. Volume I: Atmospheric Aerosol Optical Depth. October 1985 (WMO TD No. 96).

37. Air-Sea Interchange of Pollutants by R.A. Duce. September 1986 (WMO TD No. 126).

38. Summary Report on the Status of the WMO Background Air Pollution Monitoring Network as at 31 December 1985. September 1986 (WMO TD No. 136).

39. Report of the Third WMO Expert Meeting on Atmospheric Carbon Dioxide Measurement Techniques, Lake Arrowhead, California, USA, 4-8 November 1985. October 1986.

40. Report of the Fourth Session of the CAS Working Group on Atmospheric Chemistry and Air Pollution, Helsinki, Finland, 18-22 November 1985. January 1987.

41. Global Atmospheric Background Monitoring for Selected Environmental Parameters. BAPMoN Data for 1982, Volume II: Precipitation chemistry, continuous atmospheric carbon dioxide and suspended particulate matter. June 1986 (WMO TD No. 116).

42. Scripps reference gas calibration system for carbon dioxide-in-air standards: revision of 1985 by C.D. Keeling, P.R. Guenther and D.J. Moss. September 1986 (WMO TD No. 125).

43. Recent progress in sunphotometry (determination of the aerosol optical depth). November 1986.

44. Report of the Sixth Session of the WMO Executive Council Panel of Experts on Environmental Pollution, Geneva, 5-9 May 1986. March 1987.

45. Proceedings of the International Symposium on Integrated Global Monitoring of the State of the Biosphere (Volumes I-IV), Tashkent, USSR, 14-19 October 1985. December 1986 (WMO TD No. 151).

46. Provisional Daily Atmospheric Carbon Dioxide Concentrations as Measured at BAPMoN Sites for the Year 1984. December 1986 (WMO TD No. 158).

47. Procedures and Methods for Integrated Global Background Monitoring of Environmental Pollution by F.Ya. Rovinsky, USSR and G.B. Wiersma, USA. August 1987 (WMO TD No. 178).

48. Meeting on the Assessment of the Meteorological Aspects of the Third Phase of EMEP IIASA, Laxenburg, Austria, 30 March - 2 April 1987. February 1988.

49. Proceedings of the WMO Conference on Air Pollution Modelling and its Application (Volumes I-III), Leningrad, USSR, 19-24 May 1986. November 1987 (WMO TD No. 187).

50. Provisional Daily Atmospheric Carbon Dioxide Concentrations as Measured at BAPMoN Sites for the Year 1985. December 1987 (WMO TD No. 198).

51. Report of the NBS/WMO Expert Meeting on Atmospheric CO_2 Measurement Techniques, Gaithersburg, USA, 15-17 June 1987. December 1987.

52. Global Atmospheric Background Monitoring for Selected Environmental Parameters. BAPMoN Data for 1985. Volume I: Atmospheric Aerosol Optical Depth. September 1987.

53. WMO Meeting of Experts on Strategy for the Monitoring of Suspended Particulate Matter in BAPMoN - Reports and papers presented at the meeting, Xiamen, China, 13-17 October 1986. October 1988.

54. Global Atmospheric Background Monitoring for Selected Environmental Parameters. BAPMoN Data for 1983, Volume II: Precipitation chemistry, continuous atmospheric carbon dioxide and suspended particulate matter (WMO TD No. 283).

55. Summary Report on the Status of the WMO Background Air Pollution Monitoring Network as at 31 December 1987 (WMO TD No. 284).

56. Report of the First Session of the Executive Council Panel of Experts/CAS Working Group on Environmental Pollution and Atmospheric Chemistry, Hilo, Hawaii, 27-31 March 1988. June 1988.

57. Global Atmospheric Background Monitoring for Selected Environmental Parameters. BAPMoN Data for 1986, Volume I: Atmospheric Aerosol Optical Depth. July 1988.

58. Provisional Daily Atmospheric Carbon Dioxide Concentrations as measured at BAPMoN sites for the years 1986 and 1987 (WMO TD No. 306).

59. Extended Abstracts of Papers Presented at the Third International Conference on Analysis and Evaluation of Atmospheric CO_2 Data - Present and Past, Hinterzarten, Federal Republic of Germany, 16-20 October 1989 (WMO TD No. 340).

60. Global Atmospheric Background Monitoring for Selected Environmental Parameters. BAPMoN Data for 1984 and 1985, Volume II: Precipitation chemistry, continuous atmospheric carbon dioxide and suspended particulate matter.

61. Global Atmospheric Background Monitoring for Selected Environmental Parameters. BAPMoN Data for 1987 and 1988, Volume I: Atmospheric Aerosol Optical Depth.

62. Provisional Daily Atmospheric Carbon Dioxide Concentrations as measured at BAPMoN sites for the year 1988 (WMO TD No. 355).

63. Report of the Informal Session of the Executive Council Panel of Experts/CAS Working Group on Environmental Pollution and Atmospheric Chemistry, Sofia, Bulgaria, 26 and 28 October 1989.

64. Report of the consultation to consider desirable locations and observational practices for BAPMoN stations of global importance, Bermuda Research Station, 27-30 November 1989.

65. Report of the Meeting on the Assessment of the Meteorological Aspects of the Fourth Phase of EMEP, Sofia, Bulgaria, 27 and 31 October 1989.

66. Summary Report on the Status of the WMO Global Atmosphere Watch Stations as at 31 December 1990 (WMO TD No. 419).

67. Report of the Meeting of Experts on Modelling of Continental, Hemispheric and Global Range Transport, Transformation and Exchange Processes, Geneva, 5-7 November 1990.

68. Global Atmospheric Background Monitoring for Selected Environmental Parameters. BAPMoN Data For 1989, Volume I: Atmospheric Aerosol Optical Depth.

69. Provisional Daily Atmospheric Carbon Dioxide Concentrations as measured at Global Atmosphere Watch (GAW)-BAPMoN sites for the year 1989 (WMO TD No. 400).

70. Report of the Second Session of EC Panel of Experts/CAS Working Group on Environmental Pollution and Atmospheric Chemistry, Santiago, Chile, 9-15 January 1991 (WMO TD No. 633).

71. Report of the Consultation of Experts to Consider Desirable Observational Practices and Distribution of GAW Regional Stations, Halkidiki, Greece, 9-13 April 1991 (WMO TD No. 433).

72. Integrated Background Monitoring of Environmental Pollution in Mid-Latitude Eurasia by Yu.A. Izrael and F.Ya. Rovinsky, USSR (WMO TD No. 434).

73. Report of the Experts Meeting on Global Aerosol Data System (GADS), Hampton, Virginia, 11 to 12 September 1990 (WMO TD No. 438).

74. Report of the Experts Meeting on Aerosol Physics and Chemistry, Hampton, Virginia, 30 to 31 May 1991 (WMO TD No. 439).

75. Provisional Daily Atmospheric Carbon Dioxide Concentrations as measured at Global Atmosphere Watch (GAW)-BAPMoN sites for the year 1990 (WMO TD No. 447).

76. The International Global Aerosol Programme (IGAP) Plan: Overview (WMO TD No. 445).

77. Report of the WMO Meeting of Experts on Carbon Dioxide Concentration and Isotopic Measurement Techniques, Lake Arrowhead, California, 14-19 October 1990.

78. Global Atmospheric Background Monitoring for Selected Environmental Parameters BAPMoN Data for 1990, Volume I: Atmospheric Aerosol Optical Depth (WMO TD No. 446).

79. Report of the Meeting of Experts to Consider the Aerosol Component of GAW, Boulder, 16 to 19 December 1991 (WMO TD No. 485).

80. Report of the WMO Meeting of Experts on the Quality Assurance Plan for the GAW, Garmisch-Partenkirchen, Germany, 26-30 March 1992 (WMO TD No. 513).

81. Report of the Second Meeting of Experts to Assess the Response to and Atmospheric Effects of the Kuwait Oil Fires, Geneva, Switzerland, 25-29 May 1992 (WMO TD No. 512).

82. Global Atmospheric Background Monitoring for Selected Environmental Parameters BAPMoN Data for 1991, Volume I: Atmospheric Aerosol Optical Depth (WMO TD No. 518).

83. Report on the Global Precipitation Chemistry Programme of BAPMoN (WMO TD No. 526).

84. Provisional Daily Atmospheric Carbon Dioxide Concentrations as measured at GAW-BAPMoN sites for the year 1991 (WMO TD No. 543).

85. Chemical Analysis of Precipitation for GAW: Laboratory Analytical Methods and Sample Collection Standards by Dr Jaroslav Santroch (WMO TD No. 550).

86. The Global Atmosphere Watch Guide, 1993 (WMO TD No. 553).

87. Report of the Third Session of EC Panel/CAS Working Group on Environmental Pollution and Atmospheric Chemistry, Geneva, 8-11 March 1993 (WMO TD No. 555).

88. Report of the Seventh WMO Meeting of Experts on Carbon Dioxide Concentration and Isotopic Measurement Techniques, Rome, Italy, 7-10 September 1993, (edited by Graeme I. Pearman and James T. Peterson) (WMO TD No. 669).

89. 4th International Conference on CO_2 (Carqueiranne, France, 13-17 September 1993) (WMO TD No. 561).

90. Global Atmospheric Background Monitoring for Selected Environmental Parameters GAW Data for 1992, Volume I: Atmospheric Aerosol Optical Depth (WMO TD No. 562).

91. Extended Abstracts of Papers Presented at the WMO Region VI Conference on the Measurement and Modelling of Atmospheric Composition Changes Including Pollution Transport, Sofia, 4 to 8 October 1993 (WMO TD No. 563).

92. Report of the Second WMO Meeting of Experts on the Quality Assurance/Science Activity Centres of the Global Atmosphere Watch, Garmisch-Partenkirchen, 7-11 December 1992 (WMO TD No. 580).

93. Report of the Third WMO Meeting of Experts on the Quality Assurance/Science Activity Centres of the Global Atmosphere Watch, Garmisch-Partenkirchen, 5-9 July 1993 (WMO TD No. 581).

94. Report on the Measurements of Atmospheric Turbidity in BAPMoN (WMO TD No. 603).

95. Report of the WMO Meeting of Experts on UV-B Measurements, Data Quality and Standardization of UV Indices, Les Diablerets, Switzerland, 25-28 July 1994 (WMO TD No. 625).

96. Global Atmospheric Background Monitoring for Selected Environmental Parameters WMO GAW Data for 1993, Volume I: Atmospheric Aerosol Optical Depth.

97. Quality Assurance Project Plan (QAPjP) for Continuous Ground Based Ozone Measurements (WMO TD No. 634).

98. Report of the WMO Meeting of Experts on Global Carbon Monoxide Measurements, Boulder, USA, 7-11 February 1994 (WMO TD No. 645).

99. Status of the WMO Global Atmosphere Watch Programme as at 31 December 1993 (WMO TD No. 636).

100. Report of the Workshop on UV-B for the Americas, Buenos Aires, Argentina, 22-26 August 1994.

101. Report of the WMO Workshop on the Measurement of Atmospheric Optical Depth and Turbidity, Silver Spring, USA, 6-10 December 1993, (edited by Bruce Hicks) (WMO TD No. 659).

102. Report of the Workshop on Precipitation Chemistry Laboratory Techniques, Hradec Kralove, Czech Republic, 17-21 October 1994 (WMO TD No. 658).

103. Report of the Meeting of Experts on the WMO World Data Centres, Toronto, Canada, 17 - 18 February 1995, (prepared by Edward Hare) (WMO TD No. 679).

104. Report of the Fourth WMO Meeting of Experts on the Quality Assurance/Science Activity Centres (QA/SACs) of the Global Atmosphere Watch, jointly held with the First Meeting of the Coordinating Committees of IGAC-GLONET and IGAC-ACE, Garmisch-Partenkirchen, Germany, 13 to 17 March 1995 (WMO TD No. 689).

105. Report of the Fourth Session of the EC Panel of Experts/CAS Working Group on Environmental Pollution and Atmospheric Chemistry (Garmisch, Germany, 6-11 March 1995) (WMO TD No. 718).

106. Report of the Global Acid Deposition Assessment (edited by D.M. Whelpdale and M-S. Kaiser) (WMO TD No. 777).

107. Extended Abstracts of Papers Presented at the WMO-IGAC Conference on the Measurement and Assessment of Atmospheric Composition Change (Beijing, China, 9-14 October 1995) (WMO TD No. 710).

108. Report of the Tenth WMO International Comparison of Dobson Spectrophotometers (Arosa, Switzerland, 24 July - 4 August 1995).

109. Report of an Expert Consultation on 85Kr and 222Rn: Measurements, Effects and Applications (Freiburg, Germany, 28-31 March 1995) (WMO TD No. 733).

110. Report of the WMO-NOAA Expert Meeting on GAW Data Acquisition and Archiving (Asheville, NC, USA, 4-8 November 1995) (WMO TD No. 755).

111. Report of the WMO-BMBF Workshop on VOC Establishment of a "World Calibration/Instrument Intercomparison Facility for VOC" to Serve the WMO Global Atmosphere Watch (GAW) Programme (Garmisch-Partenkirchen, Germany, 17-21 December 1995) (WMO TD No. 756).

112. Report of the WMO/STUK Intercomparison of Erythemally-Weighted Solar UV Radiometers, Spring/Summer 1995, Helsinki, Finland (WMO TD No. 781).

112A. Report of the WMO/STUK '95 Intercomparison of broadband UV radiometers: a small-scale follow-up study in 1999, Helsinki, 2001, Addendum to GAW Report No. 112.

113. The Strategic Plan of the Global Atmosphere Watch (GAW) (WMO TD No. 802).

114. Report of the Fifth WMO Meeting of Experts on the Quality Assurance/Science Activity Centres (QA/SACs) of the Global Atmosphere Watch, jointly held with the Second Meeting of the Coordinating Committees of IGAC-GLONET and IGAC-ACE^{Ed}, Garmisch-Partenkirchen, Germany, 15-19 July 1996 (WMO TD No. 787).

115. Report of the Meeting of Experts on Atmospheric Urban Pollution and the Role of NMSs (Geneva, 7-11 October 1996) (WMO TD No. 801).

116. Expert Meeting on Chemistry of Aerosols, Clouds and Atmospheric Precipitation in the Former USSR (Saint Petersburg, Russian Federation, 13-15 November 1995).

117. Report and Proceedings of the Workshop on the Assessment of EMEP Activities Concerning Heavy Metals and Persistent Organic Pollutants and their Further Development (Moscow, Russian Federation, 24-26 September 1996) (Volumes I and II) (WMO TD No. 806).

118. Report of the International Workshops on Ozone Observation in Asia and the Pacific Region (IWOAP, IWOAP-II), (IWOAP, 27 February-26 March 1996 and IWOAP-II, 20 August-18 September 1996) (WMO TD No. 827).

119. Report on BoM/NOAA/WMO International Comparison of the Dobson Spectrophotometers (Perth Airport, Perth, Australia, 3-14 February 1997), (prepared by Robert Evans and James Easson) (WMO TD No. 828).

120. WMO-UMAP Workshop on Broad-Band UV Radiometers (Garmisch-Partenkirchen, Germany, 22 to 23 April 1996) (WMO TD No. 894).

121. Report of the Eighth WMO Meeting of Experts on Carbon Dioxide Concentration and Isotopic Measurement Techniques (prepared by Thomas Conway) (Boulder, CO, 6-11 July 1995) (WMO TD No. 821).

122. Report of Passive Samplers for Atmospheric Chemistry Measurements and their Role in GAW (prepared by Greg Carmichael) (WMO TD No. 829).

123. Report of WMO Meeting of Experts on GAW Regional Network in RA VI, Budapest, Hungary, 5 to 9 May 1997.

124. Fifth Session of the EC Panel of Experts/CAS Working Group on Environmental Pollution and Atmospheric Chemistry, (Geneva, Switzerland, 7-10 April 1997) (WMO TD No. 898)

125. Instruments to Measure Solar Ultraviolet Radiation, Part 1: Spectral Instruments (lead author G. Seckmeyer) (WMO TD No. 1066)

126. Guidelines for Site Quality Control of UV Monitoring (lead author A.R. Webb) (WMO TD No. 884).

127. Report of the WMO-WHO Meeting of Experts on Standardization of UV Indices and their Dissemination to the Public (Les Diablerets, Switzerland, 21-25 July 1997) (WMO TD No. 921).

128. The Fourth Biennial WMO Consultation on Brewer Ozone and UV Spectrophotometer Operation, Calibration and Data Reporting, (Rome, Italy, 22-25 September 1996) (WMO TD No. 918).

129. Guidelines for Atmospheric Trace Gas Data Management (Ken Masarie and Pieter Tans), 1998 (WMO TD No. 907).

130. Jülich Ozone Sonde Intercomparison Experiment (JOSIE, 5 February to 8 March 1996), (H.G.J. Smit and D. Kley) (WMO TD No. 926).

131. WMO Workshop on Regional Transboundary Smoke and Haze in Southeast Asia (Singapore, 2 to 5 June 1998) (Gregory R. Carmichael). Two volumes.

132. Report of the Ninth WMO Meeting of Experts on Carbon Dioxide Concentration and Related Tracer Measurement Techniques (Edited by Roger Francey), (Aspendale, Vic., Australia).

133. Workshop on Advanced Statistical Methods and their Application to Air Quality Data Sets (Helsinki, 14-18 September 1998) (WMO TD No. 956).

134. Guide on Sampling and Analysis Techniques for Chemical Constituents and Physical Properties in Air and Precipitation as Applied at Stations of the Global Atmosphere Watch. Carbon Dioxide (WMO TD No. 980).

135. Sixth Session of the EC Panel of Experts/CAS Working Group on Environmental Pollution and Atmospheric Chemistry (Zurich, Switzerland, 8-11 March 1999) (WMO TD No.1002).

136. WMO/EMEP/UNEP Workshop on Modelling of Atmospheric Transport and Deposition of Persistent Organic Pollutants and Heavy Metals (Geneva, Switzerland, 16-19 November 1999) (Volumes I and II) (WMO TD No. 1008).

137. Report and Proceedings of the WMO RA II/RA V GAW Workshop on Urban Environment (Beijing, China, 1-4 November 1999) (WMO-TD. 1014) (Prepared by Greg Carmichael).

138. Reports on WMO International Comparisons of Dobson Spectrophotometers, Parts I – Arosa, Switzerland, 19-31 July 1999, Part II – Buenos Aires, Argentina (29 Nov. – 12 Dec. 1999 and Part III – Pretoria, South Africa (18 March – 10 April 2000) (WMO TD No. 1016).

139. The Fifth Biennial WMO Consultation on Brewer Ozone and UV Spectrophotometer Operation, Calibration and Data Reporting (Halkidiki, Greece, September 1998)(WMO TD No. 1019).

140. WMO/CEOS Report on a Strategy for Integrating Satellite and Ground-based Observations of Ozone (WMO TD No. 1046).

141. Report of the LAP/COST/WMO Intercomparison of Erythemal Radiometers Thessaloniki, Greece, 13-23 September 1999) (WMO TD No. 1051).

142. Strategy for the Implementation of the Global Atmosphere Watch Programme (2001-2007), A Contribution to the Implementation of the Long-Term Plan (WMO TD No.1077).

143. Global Atmosphere Watch Measurements Guide (WMO TD No. 1073).

144. Report of the Seventh Session of the EC Panel of Experts/CAS Working Group on Environmental Pollution and Atmospheric Chemistry and the GAW 2001 Workshop (Geneva, Switzerland, 2 to 5 April 2001) (WMO TD No. 1104).

145. WMO GAW International Comparisons of Dobson Spectrophotometers at the Meteorological Observatory Hohenpeissenberg, Germany (21 May – 10 June 2000, MOHp2000-1), 23 July – 5 August 2000, MOHp2000-2), (10 – 23 June 2001, MOHp2001-1) and (8 to 21 July 2001, MOHp2001-2). Prepared by Ulf Köhler (WMO TD No. 1114).

146. Quality Assurance in monitoring solar ultraviolet radiation: the state of the art. (WMO TD No. 1180).

147. Workshop on GAW in RA VI (Europe), Riga, Latvia, 27-30 May 2002. (WMO TD No. 1206).

148. Report of the Eleventh WMO/IAEA Meeting of Experts on Carbon Dioxide Concentration and Related Tracer Measurement Techniques (Tokyo, Japan, 25-28 September 2001) (WMO TD No 1138).

149. Comparison of Total Ozone Measurements of Dobson and Brewer Spectrophotometers and Recommended Transfer Functions (prepared by J. Staehelin, J. Kerr, R. Evans and K. Vanicek) (WMO TD No. 1147).

150. Updated Guidelines for Atmospheric Trace Gas Data Management (Prepared by Ken Maserie and Pieter Tans (WMO TD No. 1149).

151. Report of the First CAS Working Group on Environmental Pollution and Atmospheric Chemistry (Geneva, Switzerland, 18-19 March 2003) (WMO TD No. 1181).

152. Current Activities of the Global Atmosphere Watch Programme (as presented at the 14th World Meteorological Congress, May 2003). (WMO TD No. 1168).

153. WMO/GAW Aerosol Measurement Procedures: Guidelines and Recommendations. (WMO TD No. 1178).

154. WMO/IMEP-15 Trace Elements in Water Laboratory Intercomparison. (WMO TD No. 1195).

155. 1st International Expert Meeting on Sources and Measurements of Natural Radionuclides Applied to Climate and Air Quality Studies (Gif sur Yvette, France, 3-5 June 2003) (WMO TD No. 1201).

156. Addendum for the Period 2005-2007 to the Strategy for the Implementation of the Global Atmosphere Watch Programme (2001-2007), GAW Report No. 142 (WMO TD No. 1209).

157. JOSIE-1998 Performance of EEC Ozone Sondes of SPC-6A and ENSCI-Z Type (Prepared by Herman G.J. Smit and Wolfgang Straeter) (WMO TD No. 1218).

158. JOSIE-2000 Jülich Ozone Sonde Intercomparison Experiment 2000. The 2000 WMO international intercomparison of operating procedures for ECC-ozone sondes at the environmental simulation facility at Jülich (Prepared by Herman G.J. Smit and Wolfgang Straeter) (WMO TD No. 1225).

159. IGOS-IGACO Report - September 2004 (WMO TD No. 1235)

160. Manual for the GAW Precipitation Chemistry Programme (Guidelines, Data Quality Objectives and Standard Operating Procedures) (WMO TD No. 1251).

161 12th WMO/IAEA Meeting of Experts on Carbon Dioxide Concentration and Related Tracers Measurement Techniques (Toronto, Canada, 15-18 September 2003).

162. WMO/GAW Experts Workshop on a Global Surface-Based Network for Long Term Observations of Column Aerosol Optical Properties, Davos, Switzerland, 8-10 March 2004 (edited by U. Baltensperger, L. Barrie and C. Wehrli) (WMO TD No. 1287).

163. World Meteorological Organization Activities in Support of the Vienna Convention on Protection of the Ozone Layer (WMO No. 974).

164. Instruments to Measure Solar Ultraviolet Radiation: Part 2: Broadband Instruments Measuring Erythemally Weighted Solar Irradiance (WMO TD No. 1289).

165. Report of the CAS Working Group on Environmental Pollution and Atmospheric Chemistry and the GAW 2005 Workshop, 14-18 March 2005, Geneva, Switzerland (WMO TD No. 1302).

166. Joint WMO-GAW/ACCENT Workshop on The Global Tropospheric Carbon Monoxide Observations System, Quality Assurance and Applications (EMPA, Dübendorf, Switzerland, 24 – 26 October 2005) (edited by J. Klausen) (WMO TD No. 1335).

167. The German Contribution to the WMO Global Atmosphere Watch Programme upon the 225th Anniversary of GAW Hohenpeissenberg Observatory (edited by L.A. Barrie, W. Fricke and R. Schleyer (WMO TD No. 1336).

168. 13th WMO/IAEA Meeting of Experts on Carbon Dioxide Concentration and Related Tracers Measurement Techniques (Boulder, Colorado, USA, 19-22 September 2005) (edited by J.B. Miller) (WMO TD No. 1359).

169. Chemical Data Assimilation for the Observation of the Earth's Atmosphere – ACCENT/WMO Expert Workshop in support of IGACO (edited by L.A. Barrie, J.P. Burrows, P. Monks and P. Borrell) (WMO TD No. 1360).

170. WMO/GAW Expert Workshop on the Quality and Applications of European GAW Measurements (Tutzing, Germany, 2-5 November 2004) (WMO TD No. 1367).

171. A WMO/GAW Expert Workshop on Global Long-Term Measurements of Volatile Organic Compounds (VOCs) (Geneva, Switzerland, 30 January – 1 February 2006) (WMO TD No. 1373).

172. WMO Global Atmosphere Watch (GAW) Strategic Plan: 2008 – 2015 (WMO TD No. 1384)

173. Report of the CAS Joint Scientific Steering Committee on Environmental Pollution and Atmospheric Chemistry (Geneva, Switzerland, 11-12 April 2007) (WMO TD No.1410).

174. World Data Centre for Greenhouse Gases Data Submission and Dissemination Guide (WMO TD No. 1416).

175. The Ninth Biennial WMO Consultation on Brewer Ozone and UV Spectrophotometer Operation, Calibration and Data Reporting (Delft, Netherlands, 31-May – 3 June 2005) (WMO TD No. 1419).

176. The Tenth Biennial WMO Consultation on Brewer Ozone and UV Spectrophotometer Operation, Calibration and Data Reporting (Northwich, United Kingdom, 4-8 June 2007) (WMO TD No. 1420).

177. Joint Report of COST Action 728 and GURME – Overview of Existing Integrated (off-line and on-line) Mesoscale Meteorological and Chemical Transport Modelling in Europe (ISBN 978-1-905313-56-3) (WMO TD No. 1427).

178. Plan for the implementation of the GAW Aerosol Lidar Observation Network GALION, (Hamburg, Germany, 27 – 29 March 2007) (WMO TD No. 1443).